JPRS L/9805

24 June 1981

USSR Report

PHYSICS AND MATHEMATICS

(FOUO 6/81)

FBIS FOREIGN BROADCAST INFORMATION SERVICE

FOR OFFICIAL USE ONLY

APPROVED FOR RELEASE: 2007/02/09: CIA-RDP82-00850R000400020044-7

NOTE

JPRS publications contain information primarily from foreign newspapers, periodicals and books, but also from news agency transmissions and broadcasts. Materials from foreign-language sources are translated; those from English-language sources are transcribed or reprinted, with the original phrasing and other characteristics retained.

Headlines, editorial reports, and material enclosed in brackets [] are supplied by JPRS. Processing indicators such as [Text] or [Excerpt] in the first line of each item, or following the last line of a brief, indicate how the original information was processed. Where no processing indicator is given, the information was summarized or extracted.

Unfamiliar names rendered phonetically or transliterated are enclosed in parentheses. Words or names preceded by a question mark and enclosed in parentheses were not clear in the original but have been supplied as appropriate in context. Other unattributed parenthetical notes within the body of an item originate with the source. Times within items are as given by source.

The contents of this publication in no way represent the policies, views or attitudes of the U.S. Government.

APPROVED FOR RELEASE: 2007/02/09: CIA-RDP82-00850R000400020044-7

JPRS L/9805

24 June 1981

USSR REPORT

PHYSICS AND MATHEMATICS

(FOUO 6/81)

CONTENTS

ACOUSTICS

UDC 534.2

DIFFRACTION OF ACOUSTIC PULSES BY ELASTIC BODIES

Moscow DIFRAKTSIYA AKUSTICHESKIKH IMPUL'SOV NA UPRUGIKH TELAKH in Russian 1979 (signed to press 10 Jul 79) pp 2-4, 238-239

[Annotation, preface and table of contents from book "Diffraction of Acoustic Pulses by Elastic Bodies", by Yaan Aleksandrovich Metsaveer, Naum Davidovich Veksler and Anatoliy Svyatoslavovich Stulov, Institute of Cybernetics, ESSR Academy of Sciences, Izdatel'stvo "Nauka", 1400 copies, 240 pages]

[Text] This book presents methods of calculating acoustic echo signals from deformable bodies, and discusses the use of these signals for determining the geometric and physical parameters of the scattering bodies. An investigation is made of acoustic echo signals from thin shells and solids of spherical, cylindrical and arbitrary shape. Strain waves in thin elastic shells are studied in the framework of equations of motion that correspond to a linear shell theory of Timoshenko type, and strain waves in solid bodies are studied in the assumption of equations of linear elasticity theory. The ambient medium is taken as unbounded, and its motion is described by equations of an ideal compressible fluid. Acoustic echo signals are calculated directly in the form of individual echo signals, algorithms being proposed both for calculating the principal terms of the quasisteady approximation of the echo signals, and for finding their frontal regions. Numerical results are given. Algorithms are described for determining the parameters of thin shells from acoustic echo signals.

The book is intended for a wide class of scientific workers, undergraduates and graduate students specializing in fields of hydroacoustics and the mechanics of a solid deformable body. Figures 44, tables 5, references 280.

Preface

This book examines problems of the theory of diffraction of acoustic waves by solids. The authors limited themselves to the linear formulation of the problem. Integral transforms constituted the principal technique, and the main goal was to study unsteady wave fields in a fluid. A systematic investigation is made of the reflected pulse, the radiated circumferential and creeping-wave pulses, and also pulses transmitted by a liquid filler, and those that arise upon incidence of an acoustic pressure pulse on an elastic body. The results of analysis of

these pulses are used to develop algorithms for determining the parameters of an elastic body from the acoustic echo signal.

The monograph examines two-dimensional diffraction problems. The problems are formulated in the first chapter. The second chapter considers problems of diffraction by bodies of spherical shape: a thin elastic shell with liquid filler, and a hollow shell of revolution with meridian close to circular. The third chapter considers problems of diffraction by solids in the shape of a circular cylinder: a thin elastic shell with liquid filler, a hollow cylindrical shell and a solid elastic cylinder. The fourth chapter considers problems of diffraction by a body of arbitrary shape. The theory of circumferential waves is generalized to a noncircular cylinder, a method of solving the problem of diffraction by the Bubnov Galerkin technique is proposed, an investigation is made of reflection of an acoustic wave from a solid elastic body, and a method is proposed for solving the unsteady problem of diffraction by solids using the method of integral boundary equations. The fifth chapter proposes an algorithm for determining the parameters of a shell from the recorded acoustic echo signal.

The book gives results obtained by the authors in research in hydroacoustics done at the Institute of Cybernetics, ESSR Academy of Sciences.

N. D. Veksler wrote sections 1-3, 5-7, 9, 11, 15; Ya. A. Metsaveer wrote sections 4, 8, 10, 13, 14, 17, 18 and also point 5.2, and parts dealing with questions relating to pulses transmitted by a filler in section 5; A. S. Stulov wrote sections 12 and 16; Yu. P. Pikk assisted in getting the results presented in sections 4 and 8; M. E. Kuster outlined the points relating to pulses transmitted by a filler in section 9; V. M. Korsunskiy assisted in getting the results of point 6.5.

The authors thank professors N. A. Alumyae, U. K. Nigul and L. Ya. Aynola for constructive discussions that helped to improve the manuscript.

Contents

6610
CSO: 1862/136

CRYSTALS AND SEMICONDUCTORS

UDC 539.2:539.89:537.621

HIGH PRESSURE PHYSICS: COLLECTION OF SCIENTIFIC PAPERS

Kiev FIZIKA VYSOKIKH DAVLENIY: SBORNIK NAUCHNYKH TRUDOV in Russian (signed to press 4 Apr 79) pp 166-168

[Abstracts of articles from book "High Pressure Physics: Collection of Scientific Papers", edited by M. V. Yegorov and V. Ya. Pekurovskiy, Donetsk Physicotechnical Institute, UkSSR Academy of Sciences, Izdatel'stvo "Naukova dumka", 1,200 copies, 168 pages]

UDC 537.312.9

TUNNELING EFFECTS IN HIGH PRESSURE PHYSICS

[Abstract of article by Galkin, A. A., Svistunov, V. M. and Belogolovskiy, M. A.]

[Text] The paper gives the results of investigations of the parameters of electron-phonon interaction of some metals and alloys at high pressure by the method of electron tunneling. Consideration is given to the possible use of the tunnel method for analyzing phase diagrams of metal systems. Measurements are made of the behavior of electron velocities in lead under hydrostatic compression. Some future prospects for development of the tunnel technique in high pressure physics are discussed. Figures 5, table 1, references 19.

UDC 538.22+536.42

SPIN WAVES AND RELAXATION PROCESSES IN MAGNETICALLY ORDERED CRYSTALS

[Abstract of article by Arkhiyezer, A. I. and Bar'yakhter, V. G.]

[Text] The paper gives a historitcal overview of spin waves and relaxation processes in magnetically ordered crystals. Basic methods are described for getting spin wave spectra and attenuation factors. Consideration is given to the investigation of the part played by other quasiparticles (electrons, phonons) in the formation of spin wave spectra. A survey is given of the most important experimental methods of studying magnetic materials, and an analysis is made of the relation between experimental and theoretical results. References 4.

UDC 538.22+536.42

SOME PROBLEMS OF MAGNETICALLY ORDERED CRYSTALS

[Abstract of article by Bar'yakhtar, V. G.]

[Text] A survey of the development of research on magnetism in the Ukraine for the past 50 years. The origin and establishment of major physical schools on magnetism is traced.

Principal attention is given to the most important fundamental results found by scientists of the Ukrainian SSR Academy of Sciences in the field of physics of magnetism. References 122.

UDC 537.311.31

DIGITAL ANALYSIS IN RESEARCH ON THE INFLUENCE THAT PRESSURE HAS ON FERMI SURFACES OF METALS

[Abstract of article by Vitchinkin, V. T., Popovich, A. I., Tsymbal, L. T. and Cherkasov, A. N.]

[Text] A bibliography is given on research in the field of physics of metals under pressure, and a method is proposed for analyzing complex oscillation recordings by using fast Fourier transformation and digital asynchronous detection. This computerization of some instrument functions enables extraction of much more complete and exact information on the periods and phases of the component harmonics. The method is verified in analysis of experiments on investigation of the Fermi surface of some metals. Figures 4, references 130.

UDC 538.22+536.42+539.89

INDUCTION OF MAGNETIC PHASES 'LATENT' IN THE REGION OF NEGATIVE PRESSURES

[Abstract of article by Zavadskiy, E. A. and Val'kov, V. I.]

[Text] A survey of experimental results that have led to the detection of "latent" states that are induced by a magnetic field, and would have arisen spontaneously only in the region of negative pressures.

Methods are described for determining the limits of lability of "latent" states, and pressure-temperature phase diagrams are given for alloys of the type $Mn_{1-x}A_xAs$, where A is cobalt or iron. The properties of the initial and induced phases are compared, and ways are indicated for practical utilization of the phenomenon.

Particular attention is given to analysis of possible mechanisms leading to the existence of "latent" ferromagnetic states. A brief outline is given of the exchange-striction and exchange-crystalline mechanisms of magnetic phase transformations. Figures 13, table 1, references 35.

UDC 539.89:539.24:539.219.3:548.4:548.53

FORMATION AND MOBILITY OF DISLOCATION BOUNDARIES IN FCC METALS UNDER HIGH PRESSURE

[Abstract of article by Zaytsev, V. I. and Presnyakov, O. V.]

[Text] A survey of research on the influence that high hydrostatic pressure has on the formation and migration of dislocation boundaries in pure fcc metals. An examination is made of the pressure dependence of physical characteristics of dislocations, and their interaction. Research results are given on dislocation structure, kinetic behavior and thermoactivation analysis in polygonization of fcc metals with different stacking defect energies under conditions of high pressure. The results are compared with theoretical models known in the literature. An examination is made of the results of investigation of kinetic principles and activation parameters during formation and growth of recrystallization centers in single-crystal and polycrystalline fcc metals with annealing under the action of high hydrostatic pressure. Figures 16, tables 5, references 47.

UDC 539.21.539.25.539.26.539.379.538.89.548.4

ORDERING OF DISLOCATION ENSEMBLES UNDER CONDITIONS OF HIGH HYDROSTATIC PRESSURE

[Abstract of article by Zaytsev, V. I., Strel'tsov, V. A. and Dobrikov, A. A.]

[Text] An examination is made of problems of mobility and interaction of dislocations. The particulars of evolution of a dislocation ensemble and paths of ordering are analyzed under conditions of high hydrostatic pressure. Data are presented that show that the ordering of dislocations is a general trend in the evolution of a dislocation ensemble under conditions of hydrostatic compression, and does not depend on type of material, degree of deformation, or the type and rate of strain. Figures 10, tables 2, references 37.

UDC 537.635:537.611.43

ELECTRON SPIN-LATTICE RELAXATION OF TRANSITION IONS IN CRYSTAL HYDRATES AT HIGH PRESSURES

[Abstract of article by Kozhukhar', A. Yu., Neylo, G. N. and Tsintsadze, G. A.]

[Text] The method of pulsed saturation of electron paramagnetic absorption lines at low temperatures is used to study the effect of deformation of paramagnetic crystal hydrates (by external hydrostatic pressure) on processes of spin-lattice relaxation of transition dopant ions. It is shown that the behavior of the energy spectrum of paramagnetic ions in crystals under pressure plays a decisive part in the rate of electron spin-lattice relaxation of direct, Raman and Orbach processes. Figures 7, references 22.

6610
CSO: 8144/1086

LASERS AND MASERS

UDC 535.14

OPEN OPTICAL RESONATORS

Moscow OTKRYTYYE OPTICHESKIYE REZONATORY in Russian 1980 (signed to press 11 Apr 80) pp 2-4, 206 - 207

[Annotation, foreword and table of contents from book "Open Optical Resonators: Some Questions of Theory and Design", by Yevgeniy Fedorovich Ishchenko, Izdatel'stvo "Sovetskoye radio", 4,000 copies, 208 pages]

[Text] The theory of single cavity open optical resonators which are widely used in quantum electronics is set forth. Resonators are treated which contain internal optical elements and an inhomogeneous medium. Considerable attention is devoted to applied methods of calculating the spatial, frequency and polarization characteristics of natural resonant modes, as well as diffraction losses. The general properties of gaussian beams and the theory of their conversion by ideal optical systems are described. The distortion of natural modes in the case of resonator misalignment is analyzed.

The book is intended for scientific workers and engineers specializing in the development and application of quantum electronic devices.

4 tables, 60 figures and 134 bibliographic citations.

Foreword

Open optical resonators play an important part in modern quantum electronics. Although optical interferometers also found widescale application previously in spectroscopy, the rapid development of optical resonator theory and engineering in recent years is due to the fact that they have proved to be an almost ideal device for producing positive feedback in lasers. The overall optical resonator and the active medium placed in its cavity can be treated as a self-oscillating system, the attenuation in which is compensated by the gain in the active medium. In this case, the resonator parameters have a substantial impact on the generated emission, to a significant extent determining its spatial-frequency, polarization and energy characteristics. At the same time, passive resonators retain their independent value (those which do not contain an active medium in their cavity). Such devices are used in engineering for spatial-frequency selection of laser radiation and as optical discriminators. Passive tunable resonator systems have become particularly widespread - so called scanning interferometers, used for the analysis of the frequency characteristics of laser radiation.

Optical resonator engineering has existed for a relatively short time [89-91]. However, considerable experimental and theoretical material has been accumulated at the present time through the efforts of domestic and foreign researchers. A specific terminology has been established, which has in many respects been borrowed from microwave engineering. The widescale proactice of the utilization of resonator systems has generated its own ways of design and planning. Thus, one can speak of the appearance of a new area of physical optics: open optical resonator theory. In treating the properties of open optical resonators, both wave and beam representations play a significant role. To understand and calculate the most fundamental characteristics of a resonator, it is necessary to draw on the techniques of wave optics. In this case, the resonator can be treated as a repeating diffraction structure. At the same time, it is reasonable and sufficient in a number of cases to limit ourselves to beam techniques, treating the resonator cavity as a periodic geometric optical system. Thus, an open optical resonator is a typical device at the frontiers of optics, which has recently been given the name of "quasi-optics".

Associated with the theory of optical resonators is the area of coherent resonator beam optics, which studies the conversion of these beams by passive external optical systems. The uniqueness of the spatial distribution of the amplitude and the necessity of accounting for the phase relationships are responsible for the definite specific features of this question. Methods of designing optical systems, developed using classical incoherent applied optics, prove to be unacceptable in the general case for resonator beams.

The results of research carried out in the department of physics of Moscow Power Engineering Institute are the basis for this book. The book is intended for scientific workers and engineers specializing in the field of the development and application of various kinds of laser systems. For this reason, special attention is devoted in the book to applied aspects of optical resonator theory. Approximate study techniques are widely used for the purpose of providing material for the design and planning of actual devices. Of course, it is impossible within a limited scope to resolve all questions of optical resonator engineering; a reasonable choice of the material is essential. The contents of the book are limited to the steady-state mode. Such questions as natural mode selection and frequency stability are not included, because of the existence of monographs [4, 5]. Moreover, based on considerations of procedural unity, the group of questions considered here is limited to the framework of linear optics. The sequence for the presentation corresponds to the principle of gradually going into greater depth in the material, something which should make the book convenient for use by students of the higher educational institutes as well.

Table of Contents

8225
CSO: 1862/126

EFFICIENCY OF FOUR-WAVE INTERACTION IN A MEDIUM WITH CUBIC NONLINEARITY

Moscow IZVESTIYA AKADEMII NAUK SSSR: SERIYA FIZICHESKAYA in Russian Vol 45, No 3, Mar 81 pp 640-643

[Article by A. I. Khizhnyak, Institute of Physics, UkSSR Academy of Sciences]

[Text] Considerable research has now been done on pairwise-opposed interaction of four beams in nonlinear media. While fairly effective wavefront reversal has been attained, there are a number of results that have not been explainable in the approximation of predetermined intensities of pumping waves. Some of these results will be theoretically analyzed in this paper.

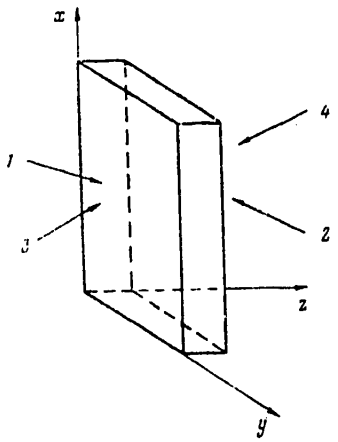

Fig. 1. Diagram of four-wave interaction: 1 and 2--pumping waves; 3--signal wave; 4--wave generated with wavefront reversal

As in Ref. 1, we will consider the interaction of four plane waves in a medium with noninertial cubic nonlinearity ($\Delta\varepsilon = \alpha|\vec{E}|^2$), but in the more general case, not assuming collinearity of the pumping waves (Fig. 1). The direction of propagation of the generated fourth wave is easily determined from the notation developed in Ref. 1 on recording and readout of dynamic holograms:

$$(\mathbf{k}_4)_{xy} = (\mathbf{k}_2 - \mathbf{k}_3 + \mathbf{k}_1)_{xy}, \qquad (1)$$

where the $(\ )_{xy}$ denotes the projection of vector $\vec{k}_i$ on the input plane of the nonlinear medium (plane xy of Fig. 1). By using condition 1 we can write a system of equations for the four interacting waves that differs from that given in Ref. 1 in the exponential cofactors ($\exp\{\pm i(\vec{k}_4 + \vec{k}_3 - \vec{k}_1 - \vec{k}_2)_z z\}$) of the final terms in the second members. These cofactors account for the phase mismatch of the waves due to disruption of space synchronism. The resultant system of equations, as before, has three integrals

$$\beta_1|a_1|^2 - \beta_4|a_4|^2 = I_1, \quad \beta_2|a_2|^2 + \beta_4|a_4|^2 = I_2, \quad \beta_3|a_3|^2 + \beta_4|a_4|^2 = I_3, \qquad (2)$$

that enable reduction of the given system to a single equation relative to any of the waves, e. g. the fourth:

$$\frac{dy}{d\zeta}=\pm 4\sqrt{(I_1+y)(I_2-y)(I_3-y)y-\left(\frac{\sigma}{4}y-\frac{\eta}{8}y^2+\Gamma_0\right)^2}, \tag{3}$$

and the expression

$$\cos\Phi\sqrt{(I_1+y)(I_2-y)(I_3-y)y}=-\frac{\sigma}{4}y+\frac{\eta}{8}y^2-\Gamma_0, \tag{4}$$

that relates the phase difference of the interacting waves $\Phi=\phi_3+\phi_4-\phi_2-\phi_1+\delta\zeta$ to their intensities. The quantity $\Gamma_0=\text{const}$ is determined from the boundary conditions. The following notation is introduced above:

$$a_i=\mathscr{E}_i(z)/|\mathscr{E}_2(d)|,\quad \beta_i=|k_i|_z/k,\quad k=2\pi/\lambda,$$
$$y=\beta_4|a_4|^2,\quad \delta=2(k_4+k_3-k_1-k_2)_z/\alpha|\mathscr{E}_2(d)|^2k,$$
$$\zeta=\alpha|\mathscr{E}_2(d)|^2kz/2B,\quad B=\sqrt{\beta_1\beta_2\beta_3\beta_4},$$
$$C=1/\beta_2+1/\beta_3-1/\beta_1-1/\beta_4,$$
$$\sigma=B[I_3(1-2C\beta_3)/\beta_3^2+I_2(1-2C\beta_2)/\beta_2^2-I_1(1+2C\beta_1)/\beta_1^2+\delta],$$
$$\eta=B\left[\sum_{n=1}^{4}\beta_n^{-2}-2C^2\right],$$

where $\mathscr{E}_i(z)$ is the slow amplitude of the field of the i-th wave; normalization to the intensity of the second wave will be convenient below.

Equation (3) coincides with equation (5) of Ref. 1 correct to the notation. Consequently the conclusions of Ref. 1 can be transferred in toto to the case of noncollinear pumping waves. The solution of equation (3) is expressed in terms of the elliptical Jacobi functions:

$$y=\frac{\alpha_3(\alpha_2-\alpha_4)-\alpha_4(\alpha_2-\alpha_3)sn^2[\mu(\zeta-D),\varkappa]}{(\alpha_2-\alpha_4)-(\alpha_2-\alpha_3)sn^2[\mu(\zeta-D),\varkappa]}, \tag{5}$$

where the α_i are the roots of the equation:

$$(I_1+y)(I_2-y)(I_3-y)y-\left(\frac{\sigma}{4}y-\frac{\eta}{8}y^2+\Gamma_0\right)^2=0, \tag{6}$$

arranged in the following order: $\alpha_1>\alpha_2>\alpha_3>\alpha_4$,

$$\mu=2/\sqrt{(\alpha_1-\alpha_3)(\alpha_2-\alpha_4)},\quad \varkappa^2=\frac{(\alpha_2-\alpha_3)(\alpha_1-\alpha_4)}{(\alpha_1-\alpha_3)(\alpha_2-\alpha_4)};$$

D is the value of ζ at $z=d$.

Since it would be difficult to analyze the solution in general form, we will take up some specific points.

1. Condition of Stimulated Emission

In this case $|a_3(0)|^2=0$, $y(d)=0$ and $y(0)=I_3$. Then $\Gamma_0=0$ and $y=0$ is a root of equation (6). Upon stimulated emission, the intensity of the fourth wave

reaches the maximum value at the output from the nonlinear medium, i. e. $y(0) = I_3$ is a root of equation (6), which leads to the condition

$$\sigma = \eta I_3/2. \tag{7}$$

Equation (7) is most simply analyzed in the case of wave incidence that is symmetric relative to the normal to the input surface of the nonlinear medium and when deviations of the pumping waves from collinearity are small, where $\beta_i \approx \beta$, $B \approx \beta^2$, $C \approx 0$, $\eta \approx 4$:

$$|a_1(0)|^2 = |a_2(d)|^2 + \delta. \tag{7'}$$

Expression (7') implies that if the pumping waves are not of equal intensity, stimulated emission is observed when the pumping waves are misaligned from collinear propagation. This result is explained in the following way [Ref. 1, 2]. As was shown in Ref. 1, due to the self-stressing of waves, the "streaks" of recorded dynamic holograms are inclined to the bisector of the angle of convergence of the recording waves. If the intensities of the pumping waves are not the same, these inclinations will differ, which mismatches Lippmann holograms, reduces the effectiveness of energy exchange between waves and makes stimulated emission impossible. On the other hand, deviation of the direction of propagation of one of the pumping waves leads to inclination of the "streaks" of holograms recorded with participation of this wave. This geometric inclination compensates for the inclination due to self-stress, which ensures conditions of stimulated emission.

2. Dependence of the Intensity of the Fourth Wave on Intensity of the Third

In the predetermined pumping wave approximation this dependence is linear [Ref. 4]. However, experimental research has shown [Ref. 5, 6] that deviation from linearity is observed where it would seem that this approximation ought to be satisfied. The deviation from linearity may lead to improper transfer of the distribution of intensities in the wave with wavefront reversal. Therefore it is important to determine the boundaries of the region of linear transfer.

Consider the case of maximum gain, where condition (7) is satisfied, but signal wave 3 at the input to the medium is different from zero, i. e. $|a_3(0)|^2 \neq 0$. Then, assuming once again for the sake of simplicity $\beta_i \approx \beta$, $B \approx \beta^2$, $C \approx 0$, $\eta \approx 4$, we get

$$|a_1(0)|^2 + |a_3(0)|^2 = |a_2(d)|^2 + \delta. \tag{7''}$$

It can be seen that attainment of maximum gain requires a completely defined relation between the intensities of the interacting waves and their direction of propagation. Relation (7'') implies in particular that in the case of collinear pumping waves ($\delta = 0$) the maximum gain is reached if the sum of the intensities of waves 1 and 3 at $z = 0$ is equal to the intensity of pumping wave 2 at $z = d$ (assuming as before that $y(d) = 0$). Under these conditions, (5) implies

$$K_i = \frac{|a_4(0)|^2}{|a_3(0)|^2} = \frac{(\sqrt{1+u}-1)\,sn^2\left[\frac{\sqrt{3}}{2} I_3(1+\sqrt{1+u})D;\ \varkappa\right]}{(\sqrt{1+u}+1)\,cn^2\left[\frac{\sqrt{3}}{2} I_3(1+\sqrt{1+u})D;\ \varkappa\right]}, \tag{8}$$

where D is the value of ζ at $z=d$, $u=16I_1I_2/3I_3^2$, $\varkappa^2=2\sqrt{1+u}/(1+u/2+\sqrt{1+u})$. If signal wave 3 and generated wave 4 are weak, i. e. $I_3 \ll I_1, I_2$, then expression (8) is transformed to

$$K_4^0=\mathrm{tg}^2(2\sqrt{I_1I_2}D), \qquad (8')$$

obtained in Ref. 4 in the predetermined pumping wave approximation. Fig. 2 shows the dependence implied by (8), the dotted straight lines corresponding to (8'). It can be seen that deviation from nonlinearity begins earlier, the larger the value reached by the transfer coefficient (8'). This is demonstrated by Fig. 3, showing K_4/K_4^0 as a function of the intensity of signal wave 3 for the same values of K_4^0 as in Fig. 2.

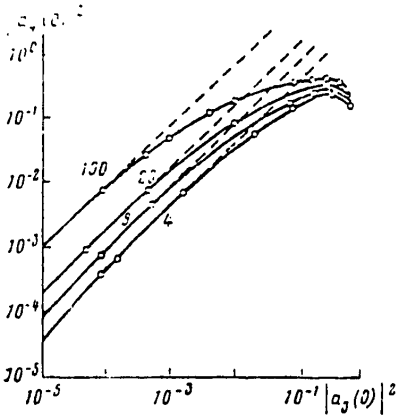

Fig. 2

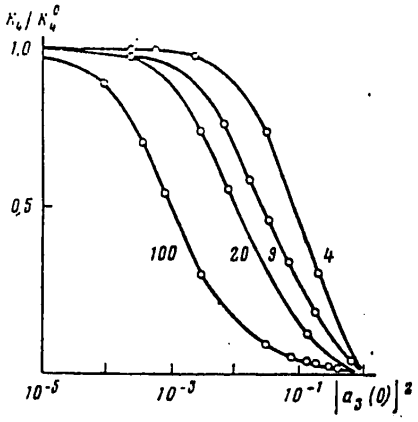

Fig. 3

Fig. 2. Intensity of the fourth wave as a function of the intensity of the third for different values of K_4^0 (indicated on the curves)

Fig. 3. Dependence of K_4/K_4^0 on the intensity of the third (signal) wave at the input to the nonlinear medium for the same values of K_4^0 as on Fig. 2

The factor leading to deviation from dependence (8') is mismatch of holographic gratings due to self-stress of the waves. If we wish to reach a higher value of K_4^0, we must increase the nonlinear phase lead on the thickness D of the medium. As a result, the self-stress increases, and consequently mismatch of the holograms sets in at a lower value of the signal wave intensity, as is demonstrated by Fig. 3.

Thus the examples considered above demonstrate the importance of accounting for self-stress of waves to determine optimum conditions of wavefront reversal in four-wave interaction.

REFERENCES

1. Soskin, M. S., Khizhnyak, A. I., KVANTOVAYA ELEKTRONIKA, Vol 7, 1980, p 42.
2. Khizhnyak, A. I., "Tezisy dokladov vtoroy Vsesoyuznoy konferentsii 'Optika lazerov'" [Abstracts of Reports to the Second All-Union Conference on Laser Optics], Leningrad, 1979, p 317.

3. Borshch, A. A., Brodin, M. S., Volkov, V. I. et al., PIS'MA V ZHURNAL TEKHNICHESKOY FIZIKI, Vol 5, 1979, p 1240.

4. Yariv, A. and Peper, D. M., OPT. LETTS., Vol 1, 1977, p 16.

5. Bloom, D. M., Liao, P. F., Economou, N. P., OPT. LETTS, Vol 2, 1978, p 58.

6. Kremenitskiy, V. V., Odulov, S. G. and Soskin, M. S., "Tezisy dokladov vtorcy Vsesoyuznoy konferentsii 'Optika lazerov'", Leningrad, 1979, p 313.

6610
CSO: 1862/165

UDC 621.373.826.038.823

DEVELOPMENT OF SMALL-SCALE INHOMOGENEITIES IN PHOTODISSOCIATION LASERS

Moscow KVANTOVAYA ELEKTRONIKA in Russian Vol 8, No 3(105), Mar 81 pp 637-639
manuscript received 4 Nov 80

[Article by V. V. Likhanskiy and A. P. Napartovich, Institute of Nuclear Power imeni I. V. Kurchatov, Moscow]

[Text] It is shown that interaction of radiation with small-scale optical inhomogeneities leads to the development of transverse structure of radiation and density due to processes of stimulated temperature scattering and stimulated Mandelstam-Brillouin scattering of light in the active medium of photodissociation lasers. Perturbations with diffraction transverse dimensions develop most rapidly.

Experimental research [Ref. 1-3] on emission of pulses with duration of ~10^{-5} s in photodissociation lasers has revealed development of small-scale inhomogeneities in the gas medium inside the resonator cavity. These inhomogeneities have shown up only when radiation is present in the active medium, and have sharply increased the divergence of emission. Qualitatively, the given effect is attributed to the fact that inhomogeneities of radiation intensity that arise during lasing lead to nonuniform heat release in the medium that changes its density, which in turn affects the distribution of intensity over the cross section of the cavity. Ref. 1 pointed out the similarity of this process to parametric excitation of sound in an active medium. Our paper is devoted to a theoretical study of this effect.

Let us note right away that this problem is similar to that of stimulated temperature scattering and stimulated Mandelstam-Brillouin scattering of light [Ref. 4, 5]. However, we should emphasize some differences in the physics of the process from formulation of the problem of stimulated scattering. In the amplifying medium of a photodissociation laser, heating causes chemical reactions of recombination. Small fluctuations of intensity lead to nonuniform distribution of iodine atoms in the medium, giving rise to fluctuations of heat release caused by a difference in the chemical reaction rates of excited and unexcited iodine atoms. We point out that these reactions may increase fluctuations of heat release due to intensity fluctuations as compared with the heat release mechanism

that is associated with direct absorption of light in the medium. In accordance with the experiments of Ref. 1-3, we will consider scattering of light through small angles with little change in the wave vector of the light in the common resonator for the main and scattered light.

Consider the simplest model of the active medium of photodissociation lasers [Ref. 1-3]. In such lasers the pumping radiation causes dissociation of RJ molecules into excited iodine atoms J* and radicals R. The fastest reactions in the active medium are the exothermic reactions

$$R+J\to RJ;\quad R+R\to R_2. \tag{1}$$

The equations that describe the change in density of molecules of J and J* take the form

$$\frac{dn_J^*}{dt}=-\left(n_J^*-n_J\right)\frac{\sigma I}{\hbar\omega}+\frac{\sigma_{RJ}I_H}{\hbar\omega_H}n_{RJ};$$
$$\frac{dn_J}{dt}=\left(n_J^*-n_J\right)\frac{\sigma I}{\hbar\omega}-\frac{n_J}{\tau_{ef}}. \tag{2}$$

Here $\sigma I/\hbar\omega$ is the probability of stimulated transition; I is the intensity of laser radiation; τ_{ef} is the effective time of the regenerating chemical reaction; I_H is the intensity of pumping radiation; $\sigma_{RJ}I_Hn_{RJ}/(\hbar\omega_H)$ is the rate of photodissociation of RJ. For the experimental conditions of Ref. 1-3, $\tau_{ef}\sim 10^{-7}$ s.

The fluctuation of heat release $\tilde{Q}$ is proportional to the fluctuation of density of iodine molecules $\tilde{Q}=\tilde{n}_Jq/\tau_{ef}$ (q is the energy released in a single act of recombination). By linearizing (2) relative to small perturbations $\tilde{n}_J^*$, $\tilde{n}_J$, $\tilde{I}$ near quasisteady solutions and taking τ_{ef} shorter than all other characteristic times, we get

$$\tilde{Q}=qn_J\sigma\tilde{I}/(\hbar\omega). \tag{3}$$

The permittivity fluctuations of the medium are due to the change in density of the gas ρ, $\tilde{\varepsilon}=(\varepsilon_0-1)\tilde{\rho}/\rho$, where ε_0 is the dielectric constant of the medium. The system of equations for fluctuations of the parameters of the medium is written as

$$\frac{1}{c_s^2}\frac{\partial^2\varphi}{dt^2}-\Delta\varphi=\tilde{Q}\frac{\gamma-1}{\gamma}\frac{1}{p_0};\quad \frac{\partial\tilde{\rho}}{\partial t}=\rho_0\Delta\varphi. \tag{4}$$

Here p_0 is pressure; c_s is the speed of sound; ϕ is the potential of velocity fluctuation ($\tilde{v}=-\Delta\phi$). System of equations (4) is analogous to material equations of Ref. 4, 5 that are used to analyze stimulated temperature scattering of the second kind and stimulated Mandelstam-Brillouin scattering. In contrast to Ref 4, 5, equations (4) omit the terms corresponding to striction forces, the electrocalorimetric effect and dissipative processes. Estimates based on the characteristic time scales taken from the experiment of Ref. 1 ($\sim 10^{-6}$ s) and scales of length from the same source (~1 mm) show that this is realistically feasible. Henceforth we will also disregard the generation of hypersound, which is strongly damped under the conditions of Ref. 1-3. This enables us to use the intensity of light averaged with respect to wavelength in (3).

The propagation of radiation in the resonator can be described by scalar parabolic equations for opposed waves. Let us assume that losses are uniformly distributed lengthwise of the active medium. In the steady state (lasing pulse duration much greater than the photon transit time in the cavity 2L/c, L is the distance between mirrors), the gain is equal to the losses, and the steady-state amplitudes of the opposed electromagnetic waves are equal to each other. The equations for perturbations of amplitudes of the electromagnetic waves take the following form:

$$\frac{\partial \widetilde{E}_+}{\partial x}+\frac{1}{c}\frac{\partial \widetilde{E}_+}{\partial t}+\frac{i}{2k}\Delta_\perp \widetilde{E}_+ + \frac{ik}{2}(\varepsilon_0-1)\frac{\widetilde{\rho}}{\rho}E_+=0;$$
$$\frac{\partial \widetilde{E}_-}{\partial x}-\frac{1}{c}\frac{\partial \widetilde{E}_-}{\partial t}-\frac{i}{2k}\Delta_\perp \widetilde{E}_- - \frac{ik}{2}(\varepsilon_0-1)\frac{\widetilde{\rho}}{\rho}E_-=0. \qquad (5)$$

Here $E_{+,-}$ are the amplitudes of opposed stationary waves; $\vec{k}$ is the wave vector of radiation; $\Delta_\perp=\frac{d^2}{dy^2}+\frac{d^2}{dz^2}$; y, z are coordinates perpendicular to the axis of the cavity.

The conditions on the mirrors take the form

$$\widetilde{E}_+(0)=\widetilde{E}_-(0), \qquad \widetilde{E}_+(L)=\widetilde{E}_-(L). \qquad (6)$$

In contrast to Ref. 4, 5, we retain diffraction effects which, as can readily be demonstrated, are important for the conditions of the experiment of Ref. 1.

In studying the stability of steady-state uniform lasing in the optical cavity, we take all perturbations proportional to $\exp(-i\Omega t+i\varkappa_\parallel x+i\varkappa_\perp r_\perp)$. From linearized equations (3)-(5) and conditions (6) we get the following dispersion equation that relates Ω to $\varkappa_\parallel, \varkappa_\perp$:

$$\left[\left(\varkappa_\parallel-\frac{\varkappa_\perp^2}{2k}\right)^2-\frac{\Omega^2}{c^2}\right]\left[\left(\varkappa_\parallel+\frac{\varkappa_\perp^2}{2k}\right)^2-\frac{\Omega^2}{c^2}\right]+2\alpha_2\frac{\varkappa_\perp^2}{2k}\left[\varkappa_\parallel^2+\frac{\Omega^2}{c^2}-\left(\frac{\varkappa_\perp^2}{2k}\right)^2\right]-$$
$$-2i\alpha_1\frac{\Omega}{c}\left[\varkappa_\parallel^2-\frac{\Omega^2}{c^2}+\left(\frac{\varkappa_\perp^2}{2k}\right)^2\right]=0. \qquad (7)$$

Here

$$\alpha_1=\frac{\varkappa^2 k(\varepsilon_0-1)|(\gamma-1)qn_j\sigma l_0}{\rho\hbar\omega}\operatorname{Re}\frac{1}{\Omega(\Omega^2-c_s^2\varkappa^2)};$$
$$\alpha_2=\frac{\varkappa^2 k(\varepsilon_0-1)(\gamma-1)qn_j\sigma l_0}{\rho\hbar\omega}\operatorname{Im}\frac{1}{\Omega(\Omega^2-c_s^2\varkappa^2)}. \qquad (8)$$

Conditions (6) give the quantization of the longitudinal wave vector of the perturbations, $\varkappa_\parallel=\pi n/L$; $n=\pm1, \pm2, \ldots$

Let us consider solutions of (7) in two cases: $|\alpha_1|\gg|\alpha_2|$ and $|\alpha_2|\gg|\alpha_1|$. At $\Omega=\Omega_0+i\Delta$, $|\Delta|\ll|\Omega_0|$ we will seek the increment of instability according to perturbation theory. The maximum increment in this case is reached with conditions

$$\Omega_0/c=\pm(\varkappa_\parallel\pm\varkappa_\perp^2/2k), \quad \Omega_0=\pm c_s\varkappa,$$

that correspond to the process of stimulated Mandelstam-Brillouin scattering and describe the laws of conservation. The maximum increment of instability can be estimated from the expression

$$\mathrm{Re}\,\Delta = \frac{1}{2\sqrt{2}}\left[\omega(\varepsilon_0-1)\frac{\gamma-1}{\rho c_s^2}qn_J\frac{\sigma I_0}{\hbar\omega}\right]^{1/3}. \tag{9}$$

In the case of a purely aperiodic build-up of perturbations ($\alpha_1 = 0$), the biggest increment is observed for perturbations with $|\varkappa_\parallel| \approx |\varkappa_\perp^2/2k|$. Assuming that $\varkappa_\parallel/k = \pm\varkappa_\perp^2/2k^2 + \delta$ ($|\delta| \ll |\varkappa_\parallel/k|$), we get the following dispersion relation

$$z(z^2+\delta^2)(z^2+\psi^2c_s^2/c^2) = \beta\psi^2\delta, \tag{10}$$

where $z = i\Omega/\omega$; $\psi^2 = (\varkappa_\perp^2+\varkappa_\parallel^2)/k^2$; $\beta = [(\varepsilon_0-1)(\gamma-1)qn_J\sigma I_0]/(\omega c^2\rho\hbar\omega)$.

Expression (10) has one real and four pairwise complex-conjugate roots. The real root of (10) is negative, which corresponds to increasing perturbations, and has its maximum absolute value under the condition $dz/d\delta = 0$, $\delta < 0$:

$$\delta = \beta\psi^2/2z(z^2+\psi^2c_s^2/c^2); \quad z = -c\beta^{1/3}/c_s\sqrt{2}.$$

The increment of instability is defined by the expression

$$\Omega = \frac{i}{\sqrt{2}}\left[\omega(\varepsilon_0-1)\frac{\gamma-1}{\rho c_s^2}qn_J\frac{\sigma I_0}{\hbar\omega}\right]^{1/3}. \tag{11}$$

Substituting parameters typical of experiments of Ref. 1-3 in expressions (9) and (11), we get a time of perturbation buildup equal to $\sim 10^{-6}$ s, which agrees well with the experimental results. Let us note that the increment of development of stimulated Mandelstam-Brillouin scattering is half that for development of stimulated temperature scattering when there is no detuning of the frequency of the scattered light.

Complete analysis of all solutions of equation (7) is difficult. The ratio of increments for the two limiting cases may be upset with arbitrary parameters. The situation may change as instability develops on the nonlinear stage, so that the question of predominance of the nature of scattering under the actual conditions of Ref. 1-3 requires further study. Let us note that in both limiting cases the optimum transverse and longitudinal wavelengths of the perturbation are interrelated as $\varkappa_\parallel \approx \varkappa_\perp^2/2k$, which has also been well confirmed experimentally [Ref. 1]. The results show that the optical inhomogeneities and increase in the divergence of light observed in the experiments of Ref. 1-3 can be attributed to development of processes of stimulated temperature scattering and stimulated Mandelstam-Brillouin scattering in the active medium of the laser.

In conclusion the authors thank L. A. Bol'shov, A. M. Dikhne and V. S. Zuyev for constructive discussion of the work.

REFERENCES

1. Zuyev, V. S., NETEMIN, V. N. and Nosach, O. Yu., KVANTOVAYA ELEKTRONIKA, Vol 6, 1979, p 875.

2. Alekhin, B. V., Borovkov, V. V., Brodskiy, A. Ya., Lazhintsev, B. V., Nor-Arevyan, V. A. and Sukhanov, L. V., KVANTOVAYA ELEKTRONIKA, Vol 7, 1980, p 1516.

3. Zuyev, V. S., Mikheyev, L. D., Startsev, A. V. and Shirokikh, A. P., KVANTOVAYA ELEKTRONIKA, Vol 6, 1979, p 2023.

4. Starunov, V. S., ZHURNAL EKSPERIMENTAL'NOY I TEORETICEHSKOY FIZIKI, Vol 57, 1969, p 1012.

5. Starunov, V. S. and Fabelinskiy, I. L., USPEKHI FIZICHESKIKH NAUK, Vol 98, 1969, p 441

6610
CSO: 1862/153

UDC 621.378.325

COPPER HALIDE LASER WITH PUMPING BY VACUUM TUBE AND THYRATRON OSCILLATORS

Moscow KVANTOVAYA ELEKTRONIKA in Russian Vol 8, No 3(105), Mar 81 pp 648-650
manuscript received 20 Jul 80

[Article by Ya. R. Abas-Ogly, S. A. Aboyan, G. V. Abrosimov, V. A. Andrianov, V. V. Vasil'tsov, B. I. Semykin, A. M. Shilin and V. N. Shulakov]

[Text] The paper describes experiments on excitation of a copper halide laser by thyratron and vacuum tube oscillators. It is proposed that several laser tubes operating synchronously in a parallel configuration be used to increase laser power. It is shown that this results in summation of both average and peak laser powers. A single laser tube gave an average lasing power of 18.5 W, and three tubes working in parallel with focusing at a single point produced a power of 30 W.

The specific energy output A_{sp} in lasers on self-limited transitions of the copper atom (when copper halides or pure copper are used as the working substance) is 30-70 $\mu J/cm^3$ [Ref. 1-3], and is obtained in lasers with a small working volume--as a rule no more than 10 cc. With a transition to working volumes of several hundred cc, A_{sp} drops by more than an order of magnitude. This can be attributed among other things to the fact that as the dimensions of the laser tube are increased there is a drop in the E/p in the discharge and in the electron temperature on the one hand, and a reduction in the discharge current density on the other. When copper halides are used, an increase in the diameter of the discharge tube past a certain size (3-4 cm) leads to contraction of the discharge. Nevertheless, the highest average emission powers are realized in lasers of large working volume [Ref. 4, 5].

There is yet another possibility of increasing laser power with an increase in the working volume, and that is to use several laser tubes operating synchronously in parallel configuration. The synchronous operation is important as it is desirable to increase both the average and peak power of emission. Synchronism of radiation of the tubes is also necessary in the case where the multiple-tube laser is to be used as an amplifier, and one of the tubes is taken as a master laser.

This paper describes preliminary results of experiments with a multiple-tube laser operating on copper halides in the self-heating mode.

Construction of the individual laser tube (Fig. 1) had to meet the following requirements: simplicity and feasibility of the manufacturing process, and accessibility of the materials to be used. The copper halide powder was scattered

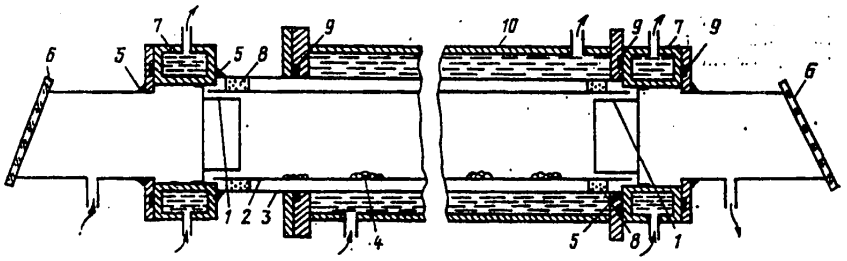

Fig. 1. Construction of the laser tube: 1--tantalum electrode rings; 2--quartz insert 3 cm in diameter; 3--quartz tube 5 cm in diameter; 4--copper halide; 5--K-400 cement; 6--output windows; 7--cooled electrodes; 8--fireclay rings; 9--silicone rubber seals; 10--cooled outer metal jacket.

uniformly over the entire discharge channel, 70 cm long, and 3 and 1.8 cm in diameter. Water cooling enabled input of high average power into the working volume of the laser without overheating of the discharge region. Let us also note that the outer metal surface of the water jacket was at the same time a coaxial shield, reducing the inductance of the discharge circuit. Thermal calculation shows that the structure is capable of draining off up to 4 kW of average power with retention of a steady temperature of 500-600°C in the discharge zone.

Excitation of laser tubes operating in parallel can be handled either by a single commutator for each tube, or by a common sufficiently powerful commutator. Thyratrons or powerful modulator tubes can be used as the commutators.

We produced an oscillator based on three TGI1-1000/25 thyratrons. The circuit was made up of three identical channels with diode-choke charging of storage capacitor C and subsequent discharge through the laser tube and thyratron. By using this oscillator we studied the capabilities of the individual laser tube from the standpoint of getting maximum average power, and also the operation of three laser tubes in a parallel configuration.

A laser tube 3 cm in diameter was excited by two channels of the oscillator. The channels operated alternately at a recurrence rate of 10 kHz, so that the total frequency of pulse excitation was 20 kHz. with copper chloride and neon as a buffer gas, a maximum average power of 18.5 W was achieved. Discharge capacitance on each channel was 1000 pF, buffer gas pressure $p_{Ne} = 5$ mm Hg, voltage across the thyratron anodes $U_{thy} = 17$ kV, efficiency of the rectifier was 0.5%. Duration of the discharge current at base was 150 ns with rise time of 25 ns. At a discharge capacitance $C = 1600$ pF, maximum current amplitude was 250 A.

In maximum-power operation of the laser, the power was about the same both with a resonator (opaque mirror and plane-parallel plate) and with a single mirror. The

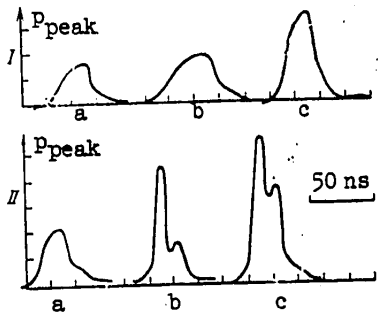

Fig. 2. Lasing pulses with parallel operation of two laser tubes (light focused to a single point): active medium CuI-Ne, p_{Ne} = 8 mm Hg; U_{thy} = 20 kV; C_1 = 1100 pF, C_2 = 1100 (I) and 1600 (II) pF; a--first tube; b--second tube; c--both tubes together

lasing pulse in the absence of the plane-parallel plate was shorter, and the peak power was higher.

A three-channel thyratron oscillator was used to excite three identical laser tubes with discharge channel diameter of 1.8 cm. The tubes were placed parallel to each other. A single common discharge circuit to all three thyratrons could be used; it was necessary to use small chokes to decouple the thyratron plates from one another. A trigger based on the TGI1-500/16 thyratron was used for simultaneous firing of the three thyratrons. The discharge currents in the tubes were time-coincident. Fig. 2 shows lasing pulses with parallel operation of two laser tubes with emission focused to a single point. Modes I and II differed in lasing power and discharge capacitance for the second tube. It can be concluded that there is practical summation of the peak emission powers. With three laser tubes an average emission power of 30 W (10 W from each tube) was obtained at a single point.

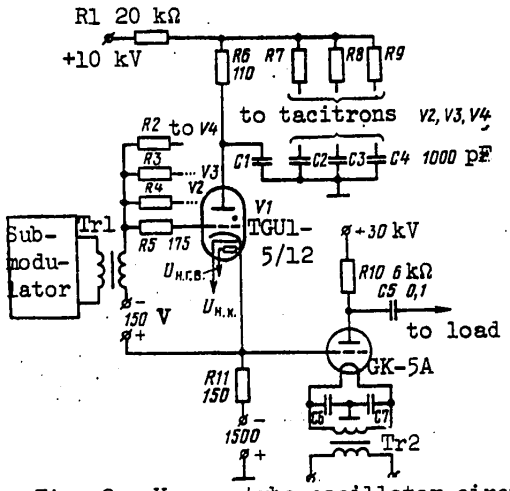

Fig. 3. Vacuum-tube oscillator circuit

Fig. 3 shows a diagram of an oscillator with GK-5A power triode. The excitation pulse to the grid of the tube was formed by four tacitrons of type TGU-5/12 operating in parallel. The capability of the tacitron to operate on frequencies up to 100 kHz enabled use of the simplest realizable method of charging the accumulator--through a resistance (the column of running cooling water).

When the oscillator operates into a linear active load of 24 Ω at an anode voltage on the lamp of 25 kV, the current in the load is 800 A. The pulse is bell-shaped with rise time of 40 ns and half-amplitude duration of about 50 ns.

When the vacuum-tube oscillator operated into the 3 cm laser tube, the current pulse had a duration of 100 ns along the base. The maximum discharge current was 300 A at a voltage of 20 kV on the anode.

At a pulse recurrence rate of 10 kHz the maximum average emission power was 10 W, rectifier efficiency was 0.6%, working substance CuCl, buffer gas neon at p_{Ne} of 2-10 mm Hg. Frequency was limited by the power of the tacitron supply source.

REFERENCES

1. Bokhan, P. A., Gerasimov, V. A., Solomonov, V. I. and Shcheglov, V. B., KVANTOVAYA ELEKTRONIKA, Vol 5, 1978, p 2162.
2. Isayev, A. A., Kazaryan, M. A., Lemmerman, T. Yu., Petrash, T. G. and Trofimov, A. N., KVANTOVAYA ELEKTRONIKA, Vol 3, 1976, p 1800.
3. Abrosimov, G. V., Vasil'tsov, V. V., in: "Tezisy dokladov devyatoy Vsesoyuznoy konferentsii po kogerentnoy i nelineynoy optike, posvyashchennoy pamyati Akademika R. V. Khokhlova" [Abstracts of Reports to the Ninth All-Union Conference on Coherent and Nonlinear Optics in Memory of Academician R. V. Khokhlov], Leningrad, 13-16 July 1978.
4. Akirtava, O. S., Dzhikiya, V. L. and Oleynik, Yu. M., KVANTOVAYA ELEKTRONIKA, Vol 2, 1975, p 1831.
5. Chen, C. J., Bhanji, A. M. and Russel, G. R., APPL. PHYS. LETTS, Vol 33, 1978, p 146.

6610
CSO: 1862/153

UDC 621.373.826.038.823

THEORETICAL INVESTIGATION OF A RING MODEL OF A SUPERSONIC CHEMICAL DF-CO_2 LASER

Moscow KVANTOVAYA ELEKTRONIKA in Russian Vol 8, No 2(104), Feb 81 pp 351-355

[Article by N. A. Konoplev, A. A. Stepanov and V. A. Shcheglov, Physics Institute imeni P. N. Lebedev, USSR Academy of Sciences, Moscow]

[Text] An investigation is made of a ring model of a supersonic chemical DF-CO_2 laser. It is shown that the ring model gives higher energy characteristics of the laser than the flat model, appreciably reduces the radiation loads on the mirrors of the optical system, and permits an increase in the initial static pressures. It is established that in the case where the factor of radial expansion of the gas flow is appreciable, the energy behavior of the laser is quite sensitive to a change in the level of initiation of the chain reaction.

1. Introduction

The idea of developing a cw chemical laser based on the process of energy transfer from excited molecules produced in a chemical reaction to cold working molecules was formulated in Ref. 1. The authors of Ref. 2, 3 were the first to carry out this idea experimentally. They made a subsonic model of a DF-CO_2 laser with the NO radical used as an initiating agent. When these radicals are mixed with fluorine molecules, atomic fluorine F is formed and serves as an active center that starts a chemical laser chain in the D_2-F_2-CO_2 mixture:

$$F+D_2 \rightarrow DF^*+D, \quad (1)$$

$$D+F_2 \rightarrow DF^*+F, \quad (2)$$

$$DF^*+CO_2(00^0 0) \rightarrow DF+CO_2(00^0 1), \quad (3)$$

$$CO_2(00^0 1)+nh\nu \rightarrow CO_2(10^0 0)+(n+1)h\nu.$$

This subsonic model of a DF-CO_2 laser was further developed in Ref. 4-8. In particular, Ref. 8 reported on attainment of an emission power of 15 kW on the large IRIS-1 laser facility. Values of chemical efficiency of about 5% and specific laser energy of about 50 J/g are typical of subsonic models of the DF-CO_2 laser. It should be noted that the low flowrates in a subsonic chemical DF-CO_2 laser considerably complicate the ejector problem, i. e. the problem of pressure recovery to atmospheric level [Ref. 9] (in the cavity region $p_{opt} \approx 15$-30 mm Hg).

Solution of this problem involves development of a supersonic laser system. A specific feature of one of the possible designs of a self-contained supersonic DF-CO_2 laser is that carbon dioxide is a product of combustion of the gas generator fuel, i. e. the laser molecules are produced during the process that heats up the mixture in the gas generator, the liberated heat being used to dissociate F_2. This arrangement was suggested by N. G. Basov, A. N. Orayevskiy and V. A. Shcheglov in 1971 (see also Ref. 10), and the model was experimentally realized in Ref. 10-12. Other models of a self-contained supersonic DF-CO_2 laser have been tested by the authors of 8, 13, 14.

In our paper for the first time an investigation is made of the peculiarities and an analysis is made of the energy capabilities of a supersonic chemical DF-CO_2 laser with cylindrical nozzle module. It is shown that a ring model with optimum geometry enables realization of quite high energy parameters of such a DF-CO_2 laser at fairly high initial pressures in the cavity region.

2. Formulation of the Problem

The cylindrical nozzle module of the supersonic chemical DF-CO_2 laser includes a large set of small coaxial plug nozzles with alternating jets of partly dissociated F_2 intermixed with D_2, CO_2 and He. The flows are discharged in the radial direction. The optical cavity is formed by mirrors of toroidal shape. The particulars of the ring model as applied to a supersonic chemical HF laser were analyzed in detail in Ref. 15-17. We note here only that the gasdynamic parameters of the flow (temperature, pressure, density) in the vicinity of the resonator can be effectively controlled by varying the radius of the cylindrical module, thus modifying the kinetic processes that form the active medium. It is shown in Ref. 16, 17 that the use of a cylindrical nozzle module is particularly advisable in the case of intense heat release in the flow since the factor of radial expansion neutralizes the reaction energy.

In the case under consideration, the equations of continuity, motion, energy and state are written respectively as

$$\rho u r = \text{const}, \tag{4a}$$

$$\rho u \frac{du}{dr} + \frac{dp}{dr} = 0, \tag{4b}$$

$$\rho u \frac{dh}{dr} - u \frac{dp}{dr} = -G_j I, \tag{4c}$$

$$p = \rho R T / W, \tag{4d}$$

where p, T, ρ, u are the pressure, temperature, density and velocity of the flow, r is the coordinate, h is the specific enthalpy of the mixture, G_j is the gain on the working transition [001]→[100] of the CO_2 molecule, I is radiation intensity, W is the molecular weight of the mixture, and R is the universal gas constant. The model of instantaneous mixing is assumed in this paper. Obviously this model is valid if the mixing length of the reagents is much shorter than the lasing zone. The system of gasdynamic equations is supplemented by the corresponding system of kinetic equations. In addition to the chain process of excitation of DF molecules (1), exchange process (2) and radiation-induced processes (3), our calculations also took account of recombination (dissociation) processes:

$$F+F+M \rightleftarrows F_2+M,$$
$$D+D+M \rightleftarrows D_2+M,$$
$$D+F+M \rightleftarrows DF+M,$$

exchange of vibrational quanta between DF and D_2:

$$DF(v)+D_2(v') \rightleftarrows DF(v-1)+D_2(v'+1),$$

relaxation of DF and D_2 molecules:

$$DF(v)+M \rightarrow DF(v-1)+M,$$
$$D_2(v)+M \rightarrow D_2(v-1)+M,$$

relaxation of deformation ν_1, symmetric ν_2 and asymmetric stretching ν_3 modes of the CO_2 molecule:

$$CO_2(v_1, v_2, v_3)+M \rightleftarrows CO_2(v_1, v_2-1, v_3)+M,$$
$$CO_2(v_1, v_2, v_3)+M \rightleftarrows CO_2(v_1-1, v_2+2, v_3)+M,$$
$$CO_2(v_1, v_2, v_3)+M \rightleftarrows CO_2(v_1-1, v_2+1, v_3)+M,$$
$$CO_2(v_1, v_2, v_3)+M \rightleftarrows CO_2(v_1, v_2+3, v_3-1)+M,$$
$$CO_2(v_1, v_2, v_3)+M \rightleftarrows CO_2(v_1+1, v_2+1, v_3-1)+M.$$

In doing specific calculations, we used the values of kinetic constants summarized in Ref. 18-20. In describing vibrational kinetics, we used the balance system of equations for average numbers of quanta of the vibrational modes [Ref. 21]. The following were assigned as external parameters in the calculations: initial pressure p, temperature T, flow velocity u_0, and molar composition of the mixture, degree of dissociation of fluorine α_F, parameters of the cylindrical nozzle module (radius r_0 and height L_a), parameters of the mirrors of the optical system (coefficients of absorption a_1, a_2 and reflection R_1, R_2). The energy characteristics were calculated on the basis of a quasi-steady state method. In typical variants we used: $T_0 = 300$ K, $u_0 = 2$ km/s, $F_2:D_2:CO_2:He=1:1:8:23$, $L_a = 100$ cm, $a_1 = a_2 = 0.02$, $R_1 = 0.98$, $R_2 = 0.85$. Some results of the calculations are given below.

3. Results and Discussion

Fig. 1 and 2 show the change in gasdynamic parameters with radius ($x = r - r_0$). As can be seen, the geometry of the nozzle module has a considerable effect on the nature of variation in Mach number M and flow temperature T. In the case of a flat nozzle, the Mach number drops rather abruptly, which is typical of a situation where heat is fed to a supersonic flow in a channel of constant cross section (the two-dimensional case was simulated in the calculations by assigning a rather large radius of the nozzle module). Higher levels of initiation had correspondingly faster fall-off in Mach number, which is apparently due to a more rapid heat release. When the factor of radial expansion is considerable, there may be a qualitative change in the distributions of Mach number and temperature in the vicinity of the resonator. When the pace of the chain reaction is relatively slow (the level of initiation is low), the flow temperature may decrease (Fig. 2) while the Mach number increases (Fig. 1). Under these conditions there is a drop in pressure and density.

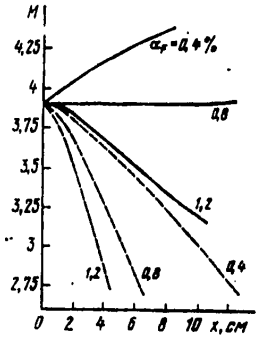

Fig. 1. Mach number as a function of radius at different levels of reaction initiation: broken lines--planar model; solid lines--ring model with radius of the nozzle module of $r_0 = 10$ cm; pressure at input to the resonator p = 100 mm Hg

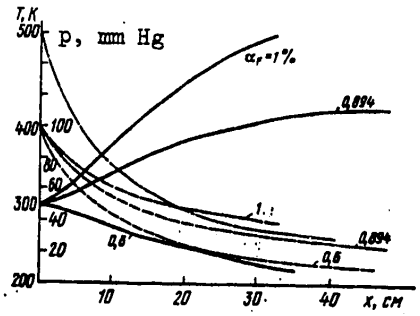

Fig. 2. Distribution of gasdynamic parameters in the laser zone at different levels of initiation α_F ($r_0 = 10$ cm); solid curves correspond to temperature T, broken curves--pressure p, dot-and-dash--gas density ρ

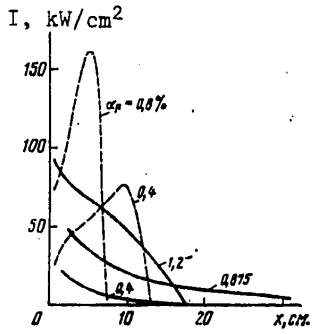

Fig. 3. Change in the intensity of laser radiation in the cavity region: solid curves--ring model with radius of nozzle module of $r_0 = 10$ cm; broken curves--planar model, p = 100 mm Hg

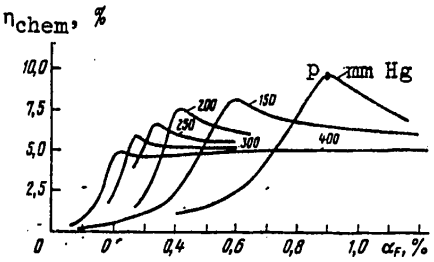

Fig. 4. Chemical efficiency of laser as a function of the level of reaction initiation at different static pressures in the resonator input; radius of nozzle module $r_0 = 10$ cm

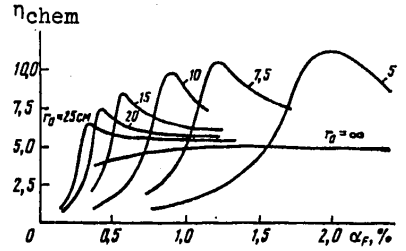

Fig. 5. Chemical efficiency of laser as a function of reaction initiation level for different radii of the nozzle module; resonator input pressure p = 100 mm Hg; curve $r_0 = \infty$--planar model

The data shown in Fig. 3-5 gives an idea of the energy capabilities of the ring model of a supersonic DF-CO_2 laser.

Fig 3 shows the distribution of laser emission intensity in the cavity region for a flat nozzle module design and in the case of the ring model. It can be seen that in the latter case the intensity variation is smoother, the lasing zone is much longer, and there is a drop in average intensity over the zone. Thus in the ring model the radiation loads on the mirrors may be considerably reduced.

Fig. 4 shows the chemical efficiency η_{chem} as a function of the initial degree of dissociation of fluorine at different pressures in the cavity input. In the qualitative respect, all curves behave alike. It is clear from the figure that for a fixed nozzle configuration and given initial pressure there is an optimum degree of fluorine dissociation where maximum energy parameters are realized. In particular, at p = 100 mm Hg the chemical efficiency is about 10%, and the specific lasing energy is about 100 J/g.

The results show that it is very important for purposes of attaining high specific laser characteristics to match the rate of development of the chain process (dependent on the level of initiation) to the pace of gasdynamic flow relief caused by radial expansion. It is worth noting that the results are sensitive to α_F at near optimum values.

Fig. 5 shows curves of chemical efficiency as a function of initiation level α_F for different values of the radius r_0 of the cylindrical nozzle module.

This figure gives a graphic demonstration of the advantages of the ring model over the flat model. The ring model doubles the efficiency of conversion of chemical energy to the energy of coherent emission.

4. Conclusions

Let us formulate the principal conclusions stemming from our analysis.

1. The use of a cylindrical nozzle module at the appropriate initial level of initiation brings about conditions for realization of high chemical efficiency (~10%), specific lasing energy (~100 J/g) and normalized laser power (~1.5 kW/cm^2).

2. In the ring model the radiation loads on the mirrors of the optical system can be appreciably reduced.

3. Use of a cylindrical module is conducive to conversion to higher static pressures in the cavity region (up to several hundred mm Hg), which is exceptionally important for solution of the ejector problem.

REFERENCES

1. Basov, N. G., Orayevskiy, A. N. and Shcheglov, V. A., ZHURNAL TEKHNICHESKOY FIZIKI, Vol 37, 1967, p 339; AIAA Selected Reprints Series, Radiative Gas Dynamics, Vol 7, 1969, p 104.

2. Cool, T. A., Stephens, R. R., J. CHEM. PHYS., Vol 51, 1969, p 5175; APPL. PHYS. LETTS., Vol 16, 1970, p 55.

3. Cool, T. A., Shirley, J. A. and Stephens, R. R., APPL. PHYS. LETTS, Vol 17, 1970, p 278.

4. Basov, N. G. et al., PIS'MA V ZHURNAL EKSPERIMENTAL'NOY I TEORETICHESKOY FIZIKI, Vol 13, 1971, p 496.

5. Shirley, J. A., Sileo, R. AN., Stephens, R. R. and Cool, T. A., AIAA Paper 71-27, 1971.

6. Brunet, H., Meabru, M., COMPT. REND. ACAD. SCI., Vol 272b, 1971, p 232.

7. Falk, T. J., REP. N. AFWL-TR-71-96, Cornell Aerospace Lab., Bufallo, N. Y., 1971.

8. Tregay, G. W., Drexhage, M. G., Wood, I. M. and Andrysiak, S. T., IEEE J., Vol QE-11, 1975, p 672.

9. Bashkin, A. S., Igoshin, V. I., Nikitin, A. I. and Orayevskiy, A. N., "Khimicheskiy lazery" [Chemical Lasers], VINITI [All-Union Institute of Scientific and Technical Information], SERIYA RADIOTEKHNIKA, Vol 8, 1975.

10. Cool, T. A., IEEE J., Vol QE-9, 1973, p 72.

11. Stregack, J. A. and Watt, W. S., IEEE J., Vol QE-11, 1975, p 711.

12. Tregay, G. W., Furner, T. E., Driskoll, R. J. and Solomon, W. C., "Fifth Conference on Chemical and Molecular Lasers", St. Louis, Mo., 1977.

13. Emanuel, G., Gaskill, W. G., Reiner, R. J., Shelton, C. and Watkins, W., IEEE J., Vol QE-12, 1976, p 739.

14. Evers, W. H., Forman, L. S. and Vieceli, J. J., IEEE J., Vol QE-11, 1975, p 711.

15. Stepanov, A. A. and Shcheglov, V. A., Preprint No 182, Lebedev Physics Institute, Moscow, 1976.

17. Stepanov, A. A. and Shcheglov, V. A., KVANTOVAYA ELEKTRONIKA, Vol 6, 1979, p 1476.

18. Kerber, R. L., APPL. OPTICS, Vol 12, 1973, p 1157.

19. Bauman, W., Blauer, J. A., Zelazny, S. W. and Solomon, W. C., APPL. OPTICS, Vol 13, 1974, p 2823.

20. Zelazny, S. W., Blauer, J. A., Wood, L., Sentman, L. H. and Solomon, W. C., APPL. OPTICS, Vol 15, 1976, p 1164.

21. Basov, N. G., Mikhaylov, V. G., Orayevskiy, A. N. and Shcheglov, V. A., ZHURNAL TEKHNICHESKOY FIZIKI, Vol 38, 1968, p 2031.

6610
CSO: 1862/124

UDC 621.375.826+535.341.08+535.37

LASING OBSERVED ON THE B-X TRANSITION OF THE XeF EXCIMER WITH KrF_2 PHOTODISSOCIATION IN MIXTURES WITH Xe

Moscow KVANTOVAYA ELEKTRONIKA in Russian Vol 8, No 2(104), Feb 81 pp 373-375

[Article by V. S. Zuyev, I. F. Isayev, A. V. Kanayev, L. D. Mikheyev, D. B. Stavrovskiy and N. G. Shchepetov, Physics Institute imeni P. N. Lebedev, USSR Academy of Sciences, Moscow]

[Text] An investigation is made of the KrF_2 absorption spectrum in the 115-190 nm region. A structureless absorption band is observed with maximum at 162 nm that has a half-width of 16 nm. It is shown that the absorption of light in this band leads to photodissociation of KrF_2 with formation of excited KrF. Lasing was observed on transition $B(v'=0)-X(v''=3)$ of the XeF excimer ($\lambda = 353$ nm) when a KrF_2-Xe-N_2-Ar gas mixture was stimulated by hard ultraviolet radiation of a high-current discharge.

In previous papers we have reported the observation of lasing on transitions B-X ($\lambda \approx 350$ nm) and C-A ($\lambda \approx 470$ nm) of the XeF excimer upon photodissociation of XeF_2 under the action of hard ultraviolet radiation of an open high-current discharge [Ref. 1, 2]. The parameters of these lasers are now being optimized. Energies of 0.15 J have been attained in the UV region [Ref. 3], and 0.5 J in the blue-green region; lasing pulse duration is 1-3 μs.

In this paper, we report on lasing observed for the first time on the B-X transition of XeF with photodissociation of KrF_2.

The absorption spectrum of KrF_2 in the region of 320-210 nm is given in Ref. 4. The absorption cross section in this region of the spectrum does not exceed $3.7 \cdot 10^{-19}$ cm^2 ($\lambda = 210$ nm). For the first time we have obtained the absorption spectrum of KrF_2 in the vacuum ultraviolet (see figure) right to 115 nm. The KrF_2 was circulated at a velocity of ~1 m/s through a nickel cell 1 cm long closed with LiF windows. The pressure of the KrF_2 in the cell was 1-5 mm Hg. The VMR-2 monochromator was used (concave grating, 600 lines/mm, R = 1 m). The source of vacuum UV was a glow discharge in hydrogen. In the region of 190-125 nm the spectrum was taken with resolution of 0.1 nm, and in the 125-115 nm region the resolution was 0.5 nm. The relative error of determination of the absorption cross section was 15%.

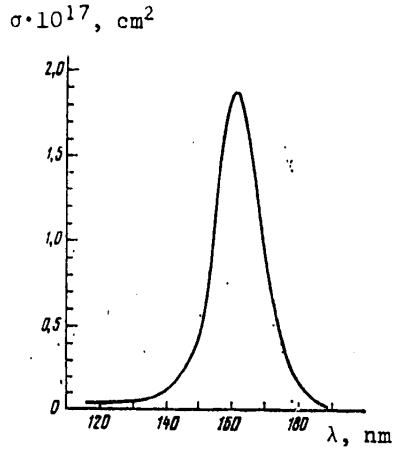

Absorption spectrum of KrF_2 in the vacuum ultraviolet

The resultant spectrum is similar to that of XeF_2, but has a number of differences. The maximum of the absorption band is located at 164 nm, and is shifted somewhat relative to the maximum of the corresponding absorption band of XeF_2 (158 nm). The bandwidths are about the same, whereas the absorption cross sections differ strongly. The cross section at the band maximum of 162 nm is 2.5-6 times less than the cross sections given in Ref. 5, 6 for the maximum of the corresponding absorption band of XeF_2. In the region that we studied, no structural bands were observed that correspond in XeF_2 to transitions to Rydberg states.

It is known that photodissociaiton of XeF_2 in the region of 124-193 nm leads to the formation of excited molecules of XeF [Ref. 7, 8]. It is also known that photodissociation of KrF_2 upon excitation on 193 nm takes place with the formation of excited KrF molecules [Ref. 9]. In studying the luminescence of gas mixtures stimulated by hard ultraviolet radiation of a high-current electric discharge, we found that photolysis of KrF_2 with the formation of KrF (B) also takes place in the region shorter than 193 nm.

To observe luminescence, the same source of pumping was used as in Ref. 1-3. A capacitor bank with capacitance of 18 μF charged to 50 kV was discharged through a tungsten wire 78 cm long located in the gas mixture. Upon excitation of a mixture of $KrF_2:CF_4:He = 2:300:1200$ mm Hg, radiation was observed with maximum at 249 nm [Ref. 10]. The thickness of the fluorescing layer was ~1 cm and corresponded to an average absorption cross section of $\sim 10^{-17}$ cm^2. Cross sections of this order of magnitude are typical of an absorption band with maximum at 162 nm. It should be noted that photolysis of KrF_2 took place in the region $\lambda > 165$ nm since the shorter-wave emission was absorbed by CF_4 [Ref. 11].

The laser experiments used a mixture of $KrF_2:Xe:N_2:Ar = 4:6:160:1500$ mm Hg. The resonator, 1.5 m in length, consisted of a spherical mirror (R ~ 3 m) and a flat mirror, the transmission factors being 2.8 and 0.6% respectively in the region of 350 nm. The resonator axis was located 12 mm from the wire. Lasing was observed on a wavelength of 353 nm, corresponding to the transition B(v' = 0)-X(v''=3) [Ref. 3]. Lasing pulse duration was 0.5 μs, energy was 1 μJ.

It is assumed that the excited molecules of XeF are formed as a result of photodissociation of KrF_2 with the formation of an excited KrF molecule and the following reaction

$$KrF^* + Xe \rightarrow XeF(B) + Kr.$$

The rate constant of this reaction has not been exactly measured, but judging from data of Ref. 12 it may be $>10^{-9}$ cm^3/s. For the analogous process

$$ArF^* + Xe \rightarrow XeF^* + Ar$$

$k = 4.5 \cdot 10^{-9}$ cm^3/s [Ref. 13].

The use of KrF_2, which has a room-temperature saturated vapor pressure of about 100 mm Hg, improves possibilities for optimization of XeF laser parameters since the pressure of XeF_2 vapor is only 3-5 mm Hg [Ref. 14].

REFERENCES

1. Basov, N. G., Zuyev, V. S., Mikheyev, L. D., Stavrovskiy, D. B. and Yalovoy, V. I., KVANTOVAYA ELEKTRONIKA, Vol 4, 1977, p 2453.
2. Basov, N. G., Zuyev, V. S., Kanayev, A. V., Mikheyev, L. D. and Stavrovskiy, D. B., KVANTOVAYA ELEKTRONIKA, Vol 6, 1979, p 1074.
3. Zuyev, V. S., Kanayev, A. V., Mikheyev, L. D. and Stavrovskiy, D. B., TRUDY FIZICHESKOGO INSTITUTA IMENI P. N. LEBEDEVA, Vol 125, 1980, p 3.
4. Makeyev, G. N., Sinyavskiy, V. F. and Smirnov, B. M., DOKLADY AKADEMII NAUK SSSR, Vol 222, 1975, p 151.
5. Nielsen, U., Schwartz, W. H. E., CHEM. PHYS., Vol 13, 1976, p 195.
6. Pysh, E. S., Jortner, J. and Rice, S. A., CHEM. PHYS., Vol 40, 1964, p 2018.
7. Brashears, H. C., Setser, D. W. and Desharteau, D., CHEM. PHYS. LETTS., Vol 48, 1977, p 84.
8. Burnham, R. and Harris, N. W., J. CHEM. PHYS., Vol 66, 1977, p 2742.
9. Burnham, R. and Searles, S. K., J. CHEM. PHYS., Vol 67, 1977, p 5967.
10. Zuyev, V. S., Kanayev, A. V., Mikheyev, L. D. and Stavrovskiy, D. B., KVANTOVAYA ELEKTRONIKA, Vol 7, 1980 p 1562.
11. Moe, G., Duncan, A. B. F., J. AMER. CHEM. SOC., Vol 74, 1952, p 3140.
12. Eden, J. G., Waynant, R. W., Searles, S. K. and Burnham, R., J. APPL. PHYS., Vol 49, 1978, p 5368.
13. Rokni, M., Jacob, J. H., Mangano, J. A. and Brochu, R., APPL. PHYS. LETTS, Vol 31, 1977, p 79.
14. Neyding, A. B. and Sokolov, V. B., USPEKHI KHIMII, Vol 43, 1974, p 2146.

6610
CSO: 1862/124

OPTICS AND SPECTROSCOPY

UDC 522.617:535.3.087

ON THE QUESTION OF PROCESSING N-SPECKLE IMAGES OF ASTRONOMICAL OBJECTS

Moscow KVANTOVAYA ELEKTRONIKA in Russian Vol 8, No 1 (103), Jan 81 pp 189-190
manuscript received 18 Jun 80

[Article by P.A. Bakut, V.N. Dudinov, K.N. Sviridov and N.D. Ustinov]

[Text] A possible approach to the solution of the problem of "seeing" through a turbulent atmosphere is treated, which is based on the recording and processing of N-speckle images of an extended astronomical object. A variant of the "speckle interferometry" method of Labeyrie is proposed, which makes it possible to reconstruct an image of an extended object undistorted by the atmosphere from the N-speckle images.

The method of obtaining and processing N-speckle images of astronomical objects for the determination of their geometrical characteristics was proposed for the first time by Labeyrie [1]. The successful experimental check of this technique [2, 3] promoted its further development. The major drawback to the method consists in the loss of the phase of the spatial spectrum of the object during processing, something which does not allow for the reconstruction of the image of the object or the determination of its angular coordinates. This substantially limits the range of applications of the method, since it makes it possible to determine the geometric characteristics of only centrosymmetrical objects from the reconstructed autocorrelation image. To retain and detect the phase of the spatial spectrum of an object and thereby expand the class of observable objects, a number of modifications of Labeyrie's method have been proposed [4].

One of these modifications is presented in this communication.

The short exposure spectrally filtered image of an astronomical object, $I_и^j$, observed through a turbulent atmosphere, can be represented in the form:

$$I_и^j = I_0 * I_{ат}^j, \qquad (1)$$

where I_0 is the true distribution of the intensity of the object; I_{at}^j is the instantaneous pulse response of the "atmosphere--telescope" system; the symbol *

indicates a convolution integral, while the superscript j indicates the ordinal number of the recorded speckle image of the object.

With the summing and corresponding normalization of N independent speckle images (1), we obtain the average image which is equivalent to a long exposure image:

$$\langle I_{\text{н}}\rangle \approx \frac{1}{N}\sum_{j=1}^{N} I_{\text{н}}^{j} = I_0 * \frac{1}{N}\sum_{j=1}^{N} I_{\text{ат}}^{j} \approx I_0 * \langle I_{\text{ат}}\rangle, \tag{2}$$

where the corner braces indicate statistical averaging.

When isoplanate objects are observed, by employing the convolution theorem for optical Fourier transforms to expressions (1) and (2), we obtain the description corresponding to them in the spatial frequency region:

$$|\tilde{I}_{\text{н}}^{j}|\, e^{i\theta_{\text{н}}^{j}} = |\tilde{I}_0|\, e^{i\theta_0} |\tilde{I}_{\text{ат}}^{j}|\, e^{i\left(\theta_{\text{а}}^{j}+\theta_{\text{т}}\right)}; \tag{3}$$

$$|\langle \tilde{I}_{\text{н}}\rangle|\, e^{i(\theta_0+\theta_{\text{т}})} = |\tilde{I}_0|\, e^{i\theta_0} |\langle \tilde{I}_{\text{ат}}\rangle|\, e^{i\theta_{\text{т}}}. \tag{4}$$

Here $|\tilde{I}_{\text{н}}^{j}|$ and $\theta_{\text{н}}^{j} = \theta_0 + \theta_{\text{т}} + \theta_{\text{а}}^{j}$ are the absolute value and phase of the spatial spectrum of the j-th image of (1) respectively; $|I_{\text{ат}}^{j}|$ and $\theta_{\text{ат}}^{j} = \theta_{\text{а}}^{j} + \theta_{\text{т}}$ are the absolute value and phase of the optical transfer function of the "atmosphere--telescope" system for the j-th image; the phase $\theta_{\text{а}}^{j}$ is due to atmospheric phase fluctuations, while the phase $\theta_{\text{т}}$ is due to telescope aberrations; $|\tilde{I}_0|$ and θ_0 are the absolute value and phase of the spatial spectrum of the object; $|\langle \tilde{I}_{\text{н}}\rangle| = \langle |\tilde{I}_{\text{н}}^{j}|\, e^{i\theta_{\text{а}}^{j}}\rangle$, and $\theta_0 + \theta_{\text{т}}$ are the absolute value and phase of the spatial spectrum of the average image (2); $|\langle \tilde{I}_{\text{ат}}\rangle| = \langle |\tilde{I}_{\text{ат}}^{j}|\, e^{i\theta_{\text{а}}^{j}}\rangle$, and $\theta_{\text{т}}$ are the absolute value and phase of the average optical transfer function of the "atmosphere--telescope" system.

It can be seen from the latter expression that within the precision of the aberration distortions of the telescope $\theta_{\text{т}}$, the phase of the spatial spectrum of an object, θ_0, can be reconstructed, by dividing the Fourier transform (4) from the average image (2) by its absolute value:

$$\langle \tilde{I}_{\text{н}}\rangle / |\langle \tilde{I}_{\text{н}}\rangle| = e^{i(\theta_0+\theta_{\text{т}})}. \tag{5}$$

It should be noted that by virtue of the rapid decline of $|\langle \tilde{I}_{\text{н}}\rangle|$ at the higher spatial frequencies in this range, the phase $\theta_0 + \theta_{\text{т}}$ may be reconstructed with considerable errors, however, this cannot have an impact on the precision in the reconstruction of the image contours of the object and its location.

To obtain the absolute value of the spatial spectrum of an object, $|\tilde{I}_0|$, in accordance with [1], the N fourier transforms (3) from the individual speckle images (1) are registered on one photographic plate with an N multiple exposure. In this case, the mean square of the absolute value of the spatial spectrum of the object image is obtained:

$$\langle|\tilde{I}_H^j|^2\rangle=|\tilde{I}_0|^2\langle|\tilde{I}_{aT}^j|^2\rangle. \tag{6}$$

To find $\langle|\tilde{I}_{at}|^2\rangle$, here, in contrast to Labeyrie's method [1], it is proposed that rather than attempting to record the N-speckle images of a point source that may not even be there, the images should be synthesized from the N-speckle images of an extended object. The synthesis concept is based on the fact that the instantaneous countours of speckle images of extended and point objects coincide and are determined by the atmospheric "seeing" spot. The difference consists only in the fact that within an atmospheric seeing spot, the size of individual spots in the image of a point source is determined by the Airy disc of the telescope, while in an image of an extended object, this size is governed by the convolution of the true distribution of object inentsity with the Airy disc of the telescope [5]. Based on this, to synthesize N independent image spots of a point source, we single out N countours of speckle images of the extended object (1) and fill them in a random fashion with the Airy discs of the telescope. Then, by performing operations on them analogous to (3) and (6), we obtain $\langle|\tilde{I}_{at}^j|^2\rangle$, and by forming the ratio between $\langle\tilde{I}_H^{j2}\rangle$ as defined by (6) and $\langle|\tilde{I}_{at}^j|^2\rangle$, we obtain the square of the absolute value of the spatial spectrum of the object:

$$\langle|\tilde{I}_H^j|^2\rangle/\langle|\tilde{I}_{aT}^j|^2\rangle=|\tilde{I}_0|^2, \tag{7}$$

from which we then ascertain $|\tilde{I}_0|$.

By subsequently realizing the inverse Fourier transform of $|\tilde{I}_0|e^{i(\theta_0+\theta_T)}$, we reconstruct the diffraction image of the object undistorted by the atmosphere.

Thus, the proposed variant substantially expands the capabilities of Labeyrie's technique [1], since it allows for its use in the absence of any kind of point sources for viewing extended objects of any geometrical shape through a turbulent atmosphere.

BIBLIOGRAPHY

1. A. Labeyrie, ASTRON. ASTROPHYS., 6, 85 (1970).

2. D.Y. Gezari, A. Labeyrie, R. Stachnic, ASTROPHYS. J., 173, 1, (1972).

3. Yu.Yu. Balega, N.A. Tikhonov, PIS'MA V ASTRON. ZHURN. [LETTERS TO THE JOURNAL OF ASTRONOMY], 3, 497, (1977).

4. P.A. Bakut, N.D. Ustinov, I.N. Troitskin, K.N. Sviridov, ZARUBEZHNAYA RADIOELEKTRONIKA [FOREIGN RADIOELECTRONICS], No 1, 3, (1976).

5. S.P. Worden, C.R. Lynds, J.W. Harvey, J. OPT. SOC. AMER., 66, 1243, 1976.

8225
CSO: 1862/123

INVESTIGATION OF HOLOGRAM ELEMENTS FOR CORRECTING THE WAVE FRONTS OF PULSE LASERS

Moscow IZVESTIYA AKADEMII NAUK SSSR: SERIYA FIZICHESKAYA in Russian Vol 45, No 3, Mar 81 pp 663-667

[Article by B. O. Mayer and D. I. Stasel'ko]

[Text] Methods of holography have opened up the capability in principle of effectively controlling the spatial structure of coherent radiation, and in particular the possibility of converting light beams with complex form of the wave front to a plane wave [Ref. 1, 2]. However, up until now the practical use of holographic correctors has been considerably limited by the low values of diffraction efficiency and by the radiation strength of the materials that are used for recording such correctors [Ref. 3]. The purpose of our work was to study the radiation strength of media that are most promising for recording hologram elements, to develop a method of producing effective hologram elements for correcting intense laser beams, and also to study the feasibility of using such elements for intracavity and extracavity correction of the wave fronts of pulse lasers.

The most promising photographic materials for producing hologram elements that correct laser beams are materials that can be used to record non-absorbing volume phase holograms since the diffraction efficiency of holograms of this type in principle can reach 100% [Ref. 4, 5]. Among such materials are type LOI-2 silver halide layers that were used in the first research on holographic correction [Ref. 6], bichromated gelatin BKhZh layers [Ref. 7] and chromated gelatin for Lippmann holography KhZhVP-1 [Ref. 8], and also Reoxan organic recording material [Ref. 9].

The radiation strength of these materials was studied in the microsecond and nanosecond ranges of light pulse duration on wavelengths of $\lambda = 0.35$, 0.53, 0.69 and 1.06 μm, and was characterized by the threshold energy density leading to destruction of the material by a single light pulse. The threshold of destruction of the material was determined visually from the visible damage of the surface or body of a specimen. The diameter of the light beam on the specimen was 1 mm. The results (see the table) show that in the free lasing mode BKhZh has the highest radiation strength (limiting energy densities up to 10 $J \cdot cm^{-2}$), while Reoxan specimens showed the best results in the Q-switched mode (limiting energy densities up to 3-7 $J \cdot cm^{-2}$).

Thresholds of destruction of holographic photo materials ($J \cdot cm^{-2}$) under the action of a single light pulse

Material	τ_p = 15-20 ns				τ_p=350-400 μs
	λ = 0.35 μm	0.53 μm	0.69 μm	1.06 μm	0.69 μm
KhZhVP-1	0.6-1.0	1.3-1.6	1.4-1.6	2.0-2.5	70-100
BKhZh, Lin method	0.6-1.0	1.3-1.6	1.8-2.0	4.0-4.5	90-110
Bleached LOI-2			0.6-1.0		
Reoxan	0.2-0.6	1.0-2.0	2.9-3.1	7.0-7.5	25-30
K8 glass			15-16		400-600

Let us also note that the principal fact that limits the radiation strength of Reoxan in the monopulse lasing mode is the defective nature of the surface of the material due to mechanical finishing. Actually, immersion of Reoxan increases its radiation strength to 6-10 $J \cdot cm^{-2}$ on λ = 0.69 μm.

Layers of various kinds of chromated gelatin and Reoxan are insensitive to the radiation of pulse lasers that emit in the red and infrared regions of the spectrum. At the same time, silver halide layers that are not resistant to the action of radiation loads have high photosensitivity to radiation pulses in these spectral bands [Ref. 10]. With this in mind, we produced hologram elements for correcting laser beams in the red and infrared by a technique in which holograms made originally on silver halide emulsions in the red and infrared were recopied onto chromated gelatin emulsions with photosensitivity in the blue-greed region of the spectrum [Ref. 11]. The copied elements produced in this way were then used to correct the initial light beam.

The initial hologram elements were recorded on IAE photographic plates sensitized to the red region of the spectrum, and the copies were made on BKhZh layers prepared by the Lin method [Ref. 7] using FP-R photographic plates as the initial material. Copying was done with argon laser radiation on λ = 0.49 μm by an interference method with the original and copy in direct contact [Ref. 11]. Recording was accomplished by interference of the wave reconstructed by the original and the wave passing through the original without scattering. Contact copying eliminated the influence of space-time coherence of the radiation source on the quality of the copy, as well as avoiding the phase distortions of the copy caused by nonuniformity of diffraction efficiency over the cross section of the original.

A study of the way that the diffraction efficiency of the copies depended on that of the original showed that this copying process can give hlolgram elements with efficiency up to 70-80% if the diffraction efficiency of the original exceeds 15% and the total flux of light scattered by the original does not exceed 3%. An increase in light scattering of the original layer to 10% limited the diffraction efficiency of the hologram element copies to 60%.

The experiments on holographic correction of distortions of active elements were done with inhomogeneous ruby crystals 16 mm in diameter and 240 mm long pumped by the GOR-300 laser illuminator. The single-pass weak-signal gain under the conditions of the experiment reached 30.

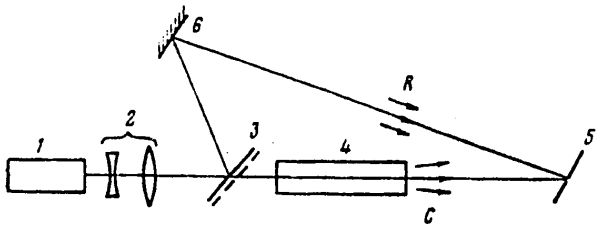

Fig. 1. Diagram of hologram element recording: 1--pulsed ruby laser; 2--30x telescope; 3--semitransparent mirror; 4--ruby crystal to be corrected; 5--hologram; 6--mirror

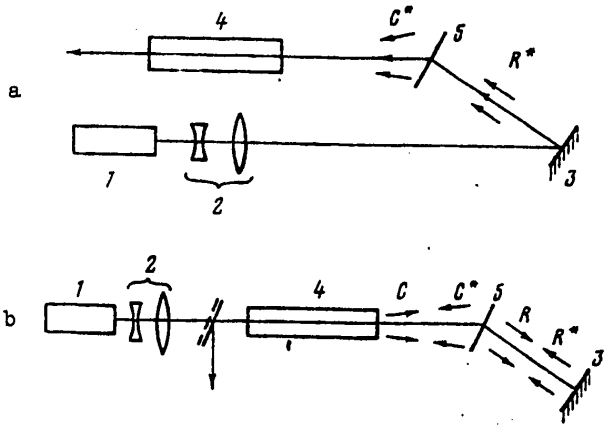

Fig. 2. Diagram of use of hologram elements for wavefront reversal in amplifier systems: a--single-pass; b--double-pass; 1--master laser; 2--telescope; 3--mirror; 4--ruby crystal to be corrected; 5--hologram element

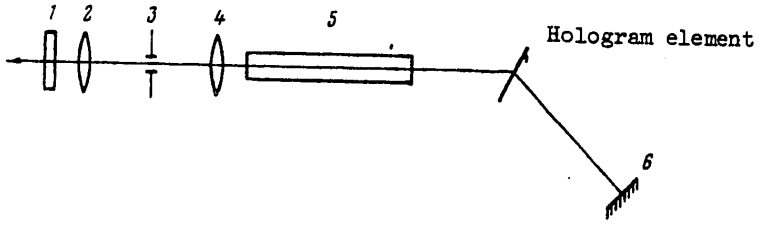

Fig. 3. Diagram of laser with hologram corrector in the optical cavity: 1--flat output mirror; 2-4--space filter system; 5--active element; 6--flat opaque mirror

A diagram of the recording of hologram element originals is shown in Fig. 1. The source of radiation was a ruby laser with unstable resonator working in the free lasing mode. The use of highly uniform ruby crystals grown by the method of the

State Optical Institute [Ref. 12] gave a radiation energy of up to 3 J with half-width divergence of 1' and coherence length of 10 cm. Telescope 2 with 30x magnification was used to produce a plane wave with half-width divergence of 30" that was sent to holographic interferometer 3-7 containing the ruby crystal 4 to be corrected. The diffraction of the hologram element originals was 15-20% after bleaching, while that of their copies on BKhZh was 40-44%, which was due to the high level of light scattering of the originals, reaching 17%.

These hologram elements were used for compensation of optical distortions of ruby crystals both in the amplifier system and in the optical cavity of the laser during operation in the free lasing mode with energy of the corrected radiation from 1 to 4 J. Systems with wavefront reversal were studied in the amplifier (see Fig. 2) like those proposed in Ref. 13, 14, and also an arrangement with the hologram element placed at the output of the amplifier [Ref. 3].

In Fig. 2a, the hologram element is placed at the input to the amplifier and shapes a light beam from the radiation of the master laser with a wavefront that is the conjugate of that passed through the amplifier when the hologram element is recorded, and in the diagram of Fig. 2b the hologram element was used for reversal of the wavefront through a two-pass amplifier. An advantage of the arrangement in Fig. 2a as compared with the two-pass scheme is resistance to self-excitation of the amplification stage and of the amplifier-master laser system. On the other hand, this scheme ensures more uniform distribution of intensity at the amplifier output as compared with the arrangement of Ref. 3 thanks to wavefront reversal through the amplifying medium, and as compared with the scheme of Fig. 2b due to the absence of amplitude distortions of the beam that reconstructs the inverted wave front.

Photometry of the distributions of intensity of amplified radiation in the far zone showed that the divergence of corrected beams corresponded to the divergence of the reference wave (~30") only when the hologram element was placed at the output of the amplifier. In the case of systems with wavefront reversal the divergence of the corrected radiation increased by a factor of 1.5-2, which was due to inaccuracy of formation of the wave conjugate to the reference wave under the experimental conditions. Calorimetric measurements showed that at least 60% of the energy of the corrected light beams was concentrated in an angle of 2' in all the investigated arrangements. The half-width divergence of the corrected beams reached ~30', and was due to considerable optical inhomogeneities in the ruby crystals that were used, with dimensions of the order of several tens of micrometers. The axial brightness of the corrected beams increased in the case of single-pass configurations by 300-400 times, and in the two-pass amplifier by 200 times as compared with the case where correction was not used.

The hologram element originals were recorded and the beams were corrected by hologram element copies under conditions where the ultraviolet component of radiation of the pumping lamps was cut out in the amplification stage, which according to Ref. 15 nearly eliminated the influence of the dynamics of the profile of optical distortions induced by pumping radiation in the ruby crystal of the amplifier. In the absence of filtration, the divergence of the corrected beams was 6-8'. The accuracy of placement of the hologram element relative to the beams to be corrected was determined by the nature of the optical inhomogeneity of the ruby crystals, and was about 1/5 of the mean size of intensity spots in the light beam

passed through the ruby element. An increase in the transverse shift of the hologram element to the mean size of the spots (50 μm) was accompanied by a reduction in the axial brightness of the corrected beam by a factor of 2-4.

A diagram of the laser with hologram element in the optical cavity is shown in Fig. 3. Space filtration system 2-4 formed a plane wave on output mirror 1. The hologram element in this arrangement operates analogously to the amplifier arrangement in Fig. 2b. Use of the hologram corrector in the laser caivty led to an increase in the axial brightness of radiation of up to five-fold as compared with a cavity without a corrector, and with equivalent transmission losses of 60% (see Fig. 4). The increase in axial brightness in the given experiment was limited by the minimum diameter of the irises used in the cavity, and also by the light scattering of the hologram element.

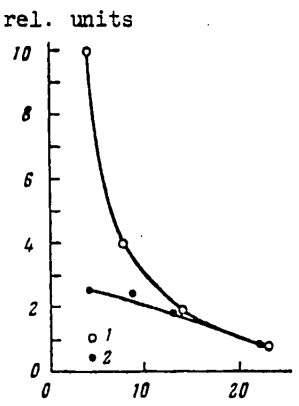

Fig. 4. Axial brightness of stimulated emission as a function of angular size of the iris in the optical cavity: 1--with hologram element; 2--without hologram element

Thus hologram elements enable efficient correction of light beams in both the emission and amplifier stages of laser systems. An important feature of such correctors is the fact that their properties are independent of the power density of the light beams, which in a number of cases enables expansion of the field of application of hologram elements as compared with dynamic correctors that are formed in nonlinear media, since in these latter the conditions of effective correction are brought about as a rule in comparatively narrow power ranges (over no more than one or two orders of magnitude) [Ref. 16, 17].

REFERENCES

1. Bondarenko, M. D., Gnatovskiy, A. V. and Soskin, M. S., DOKLADY AKADEMII NAUK SSSR, Vol 187, 1969, p 538.

2. Soskin, M. S., Bondarenko, M. D. and Gnatovskiy, A. V., PIS'MA V ZHURNAL EKSPERIMENTAL'NOY I TEORETICHESKOY FIZIKI, Vol 14, 1971, p 27.

3. Soskin, M. S., in: "Materialy chetvertoy Vsesoyuznoy shkoly po golografii" [Materials of the Fourth All-Union School on Holography], Leningrad, 1973, p 231.

4. Kogelnik, H., THE BELL SYSTEM TECHNICAL JOURNAL, Vol 48, 1969, p 2909.

5. Sidorovich, V. G., in: "Opticheskaya golografiya i yeye primeneniya" [Optical Holography and its Applications], Leningrad, "Nauka", 1977, p 4.

6. Bondarenko, M. D., Gnatovskiy, A. V. and Soskin, M. S., UKRANSKIY FIZICHESKIY AHURNAL, Vol 14, 1969, p 1930.

7. Lin, L. H., APPLIED OPTICS, Vol 8, 1969, p 963.

8. Zagorskaya, Z. A. and Shevchenko, S. B., in: "Registriruyushchiye sredy dlya izobretatel'noy golografii i kinematografii" [Recording Media for Selective Holography and Motion Picture Photography], Leningrad, "Nauka", 1979, p 114.

9. Sukhanov, V. I., Lashkov, G. I., Petnikov, A. Ye. et al., in "Opticheskaya golografiya" [Optical Holography], Leningrad, "Nauka", 1979, p 24.

10. Collier, R., Burckhardt, C., Lin, L., "Opticheskaya golografiya", Moscow, "Mir", 1973.

11. Lin, L. H., Doherty, E. T., APPLIED OPTICS, Vol 10, 1971, p 1314.

12. Musatov, M. M., OPTIKO-MEKHANICHESKAYA PROMYSHLENNOST', No 8, 1975, p 36.

13. Anan'yev, Yu. A., TRUDY GOSUDARSTVENNOGO OPTICHESKOGO INSTITUTA IMENI S. I. VAVILOVA, Vol 42, 1975, p 3.

14. Nosach, O. Yu., Popovichev, V. I., Ragul'skiy, V. V. and Fayzulov, F. S., PIS'MA V ZHURNAL EKSPERIMENTAL'NOY I TEORETICHESKOY FIZIKI, Vol 16, 1972, p 617.

15. Anan'yeva, G. V., Vasil'yeva, V. I., Danilov, S. V. et al., "Tezisy dokladov tret'yey Vsesoyuznoy konferentsii po golografii" [Abstracts of Reports to the Third All-Union Conference on Holography], Leningrad, 1978, p 153.

16. Mayer, B. O., Stasel'ko, D. I. and Churayev, A. L., "Tezisy dokladov vtory Vsesoyuznoy konferentsii 'Optika lazerov'" [Abstracts of Reports to the Second All-Union Conference on Laser Optics], Leningrad, 1980.

17. Lesnik, S. A., Soskin, M. S. and Khizhnyak, A. I. "Tezisy dokladov pervoy Vsesoyuznoy konferentsii 'Problemy upravleniya parametrami lazernogo izlucheniya'" [Abstracts of Reports to the First All-Union Conference on Problems of Controlling Laser Parameters], Tashkent, Part 1, 1978, p 119.

6610
CSO: 1862/165

UDC 621.378.535.3.087

METHODS OF EVALUATING THE CAPABILITIES OF OPTIMUM RECEPTION IN DETECTING ASTROPHYSICAL OBJECTS THROUGH A TURBULENT ATMOSPHERE

Moscow KVANTOVAYA ELEKTRONIKA in Russian Vol 8, No 2(104), Feb 81 pp 341-346

[Article by P. A. Bakut, K. N. Sviridov and N. D. Ustinov]

[Text] Probability densities are found for the square-law functionals formed upon optimum reception for real conditions of astrophysical observations with consideration of quantum effects and recording noises. These distributions are used as a basis in studying the detection characteristics of optimum reception, and an examination is made of a procedure for evaluating the capabilities of optimum reception in detecting astrophysical objects observed through a turbulent atmosphere.

Introduction

Astrophysical objects of observation are point sources (not resolvable by telescope) and extended sources of incoherent broad-band light. It was shown in our previous paper [Ref. 1] that the statistics of photocounts of optimum reception of incoherent broad-band light depends appreciably on the fluctuations of the radiation caused by the turbulent atmosphere. In this connection, the presence of atmospheric phase fluctuations not only alters the form of the probability density functional produced in optimum reception [Ref. 2], but is also detrimental to its energy characteristics. In this paper we find a quantitative estimate of the influence that these changes have on the detection characteristics of optimum reception, and examine methods of estimating the potential capabilities of detection of objects through the turbulent atmosphere.

1. Quantum Statistics of Photocounts of Optimum Reception Under Real Conditions of Astrophysical Observations

Before proceeding to the calculation and analysis of the detection characteristics of optimum reception, let us evaluate the major parameters of its probability distributions under real conditions of astrophysical observations. In order to detect astrophysical objects, it is necessary to know their integrated emission characteristics.

The principal integral characteristic that can be determined in the course of observation is the illuminance produced on the earth by radiation of a given

astrophysical object. In astrophysics, instead of the illuminance from the object, we usually make use of the concept of luminosity of the object expressed in stellar magnitudes m related to the luminance E in luxes on the basis of the Weber-Fechner law [Ref. 3] by the logarithmic function $m = m_0 - 2.5 \log E$, where $m_0 = -13^m.84$ is the stellar magnitude corresponding to one lux.

Hereafter we will limit our discussion to objects with average luminosity ranging from 5^m to 15^m. The illuminance produced by background radiation in the plane of the reception aperture of the telescope is also measured in stellar magnitudes. The minimum luminosity of the starry sky on a moonless night is 22^m from a square second of arc [Ref. 4]. When the moon is shining the background radiation increases, and may reach 16^m or more. Therefore in evaluating the potential capabilities we will assume a range of variation of 16^m-22^m in the average luminosity of the starry sky at night.

The concept of the phase space of a signal [Ref. 5] is introduced to describe an optical signal characterized by dependence on coordinates and time. This space has mM degrees of freedom, where m and M are respectively the number of temporal and spatial elements of resolution of the processing system. The average number of photoelectrons that can be detected in a space-time element of resolution is called the degeneracy parameter, and is denoted by $\delta = \bar{n}/mM$. Depending on the values of this parameter, we distinguish degenerate ($\delta \gg 1$) and nondegenerate ($\delta \ll 1$) signals. Let us determine this parameter under real conditions of astrophysical observations. To do this, we first determine the number of space-time elements of resolution mM.

Observations are almost always carried out under conditions where the object is not resolved by the reception aperture of the telescope, and is observed as a point source; in this case the number of spatial elements of resolution is M = 1. The number of temporal elements of resolution m is determined by the product of observation time T multiplied by the passband of the processing system Δf. The problem of selection of T and Δf under conditions of atmospheric "seeing" is considered in detail in Ref. 2, and in this connection we will use the following values of the passband: $\Delta f = 10^{11}$ Hz ($\Delta\lambda = 0.1$ nm); $\Delta f = 10^{13}$ Hz ($\Delta\lambda = 10$ nm); $\Delta f = 5 \cdot 10^{13}$ Hz ($\Delta\lambda = 50$ nm); T = 0.001, 0.02, 0.2 and 10 s.

With consideration of this, the number of temporal degrees of freedom of the recorded signal ranges from $m_{min} = T_{min}\Delta f_{min} = 10^8$ to $m_{max} = T_{max}\Delta f_{max} = 5 \cdot 10^{14}$. Let us now determine the average number of signal $\bar{n}_C$, background $\bar{n}_\Phi$ and dark $\bar{n}_T$ photoelectrons under real conditions of astrophysical observations. We calculate $\bar{n}_C$ and $\bar{n}_\Phi$ from the known formulas [Ref. 6]

$$\bar{n}_c = 3{,}8 \cdot 10^{4-0{,}4m_c} \gamma D_T^2 \tau_{атм} \tau_{опт} T \Delta\lambda; \quad (1)$$

$$\bar{n}_\Phi = 1{,}3 \cdot 10^{15-0{,}4m_\Phi} \gamma (D_T/F_T)^2 d^2 \tau_{опт} T \Delta\lambda, \quad (2)$$

Here $\gamma = \gamma(\omega) = 0.1$ is the quantum efficiency of the multislit photocathode in the visible region of the spectrum, m_C is the luminosity of the object in stellar magnitudes, m_Φ is the luminosity of the starry night sky, D_T is the diameter of the telescope aperture, $\tau_{атм}$ is the coefficient of transmission of light in the atmosphere, $\tau_{опт}$ is the transmission coefficient for light in the optical system, d is the diameter of the Airy spot of the telescope in the image plane, F_T is the focal length of the telescope.

TABLE 1

m_c	$D_T=1.3$ м											
	$T=10^{-3}$ s			$T=0.02$ s			$T=0.2$ s			$T=1$ s		
	Δλ, nm			Δλ, nm			Δλ, nm			Δλ, nm		
	0.1	10	50	0.1	10	50	0.1	10	50	0.1	10	50
	$\bar{n}_c$											
5	4,7	470	2350	94	9400	47000	940	94000	470000	47000	$47\cdot10^5$	$235\cdot10^5$
7	0,74	74	370	14,8	1480	7400	148	14800	74000	7400	$7,4\cdot10^5$	$37\cdot10^5$
9	0,118	11,8	59	2,36	236	1180	23,6	2360	11800	1180	118000	590000
10	0,047	4,7	23,5	0,94	94	470	9,4	940	4700	470	47000	235000
11	0,019	1,9	9,5	0,38	38	190	3,8	380	1900	190	19000	95000
13	0,003	0,3	1,5	0,06	6	30	0,6	60	300	30	3000	15000
15	0,00047	0,047	0,235	0,0094	0,94	4,7	0,094	9,4	47	4,7	470	2350
m_Φ	$\bar{n}_\Phi$											
16	0,0089	0,89	4,45	0,178	17,8	89	1,78	178	890	89	8900	44500
17	0,0035	0,35	1,75	0,07	7	35	0,7	70	350	35	3500	17500
18	0,0014	0,14	0,7	0,028	2,8	14	0,28	28	140	14	1400	7000
19	0,00056	0,056	0,28	0,011	1,1	5,6	0,11	11	56	5,6	560	2800
20	0,00022	0,022	0,11	0,0044	0,44	2,2	0,044	4,4	22	2,2	220	1100
21	$89\cdot10^{-6}$	0,0089	0,0445	0,00178	0,178	0,89	0,0178	1,78	8,9	0,89	89	445
22	$35\cdot10^{-6}$	0,0035	0,0175	0,0007	0,07	0,35	0,007	0,7	3,5	0,35	35	175

The results of calculations of $\bar{n}_C$ and $\bar{n}_\Phi$ from formulas (1) and (2) at $D_T/F_T = 1/30$, $d = 0.02$ mm, $\lambda = 0.5$ μm, $\tau_{ATM} = 0.7$, $\tau_{OPT} = 0.5$ are summarized in Table 1. It can be seen that $\bar{n}_C$ in a spatial element of resolution ($M = 1$) fluctuates from $\bar{n}_C^{min} = 4.7\cdot10^{-3}$ to $\bar{n}_C^{max} = 2.35\cdot10^{7}$, while $\bar{n}_\Phi$ ranges from $\bar{n}_\Phi^{min} = 3.5\cdot10^{-6}$ to $\bar{n}_\Phi^{max} = 4.45\cdot10^{4}$. It is interesting to compare these values with the average number of dark photoelectrons from an element of resolution for the corresponding processing time. In astrophysics, television and photographic equipment are used in combination with an image converter as light receivers for observation of cosmic objects. The use of an image converter considerably improves the sensitivity of the processing system; however, the contrast of the recorded image in this case depends on the dark current of the image converter due to thermionic emission of its input photocathode. If the number of dark photoelectrons exceeds the number of background photoelectrons, this reduces the contrast of the image on the image converter screen as compared with its contrast against the night sky. To avoid this, the photocathode of the image converter is cooled, resulting in a number of dark photoelectrons equal to 10^3 from 1 cm^2 of the surface of a multislit photocathode in 1 s at +10°C. Then from an element of resolution $d = 0.02$ mm in time $T = 10^{-3}$ s, $\bar{n}_T = 4\cdot10^{-6}$, which is considerably less than $\bar{n}_\Phi^{min} = 3.5\cdot10^{-4}$. Hence it is clear that dark currents can be disregarded with appropriate cooling of the photocathode. Moreover, we note that in the spatial element of resolution $\bar{n}_C + \bar{n}_\Phi \ll m$, i. e. a broad-band light signal from astrophysical objects is nondegenerate. In this connection, the probability distributions of square-law functionals (56) and (57) derived in [Ref. 1] are approximated with a high degree of accuracy by the following Poisson distributions:

in the presence of a useful signal

$$P_{сш}(n) = (\bar{n}_c + \bar{n}_\phi)^n e^{-(\bar{n}_c + \bar{n}_\phi)}/n! = (A+B)^n e^{-(A+B)}/n! \tag{3}$$

In the absence of a useful signal

$$P_ш(n) = \bar{n}_\phi^n e^{-\bar{n}_\phi}/n! = A^n e^{-A}/n!, \tag{4}$$

where

$$\bar{n}_c = B = mqq_a/(1+q);\ \bar{n}_\phi = A = mq/(1+q);\ \bar{n}_c/\bar{n}_\phi = B/A = q_a. \tag{5}$$

Here q, q_a is the signal-to-noise ratio in a space-time element of resolution of the processing system with and without atmospheric distortions respectively.

Before going on to calculation of the detection characteristics from the resultant distributions (3) and (4), let us make a few comments about the relation between q and q_a. In the presence of atmospheric phase distortions, the resolution of the atmosphere-telescope system is determined by the spatial correlation coefficient R_θ of the field distorted by the atmosphere rather than by D_T. In this connection, the image of each point of an object in an element of resolution of the reception aperture $\sim(\lambda F_T/D_T)^2$ is blurred into region $\sim(\lambda F_T/R_\theta)^2$, and $\bar{n}_c$ in a spatial element of resolution is reduced by a factor of $N = (D_T/R_\theta)^2$. Thus we can say that q_a is related to q by the simple expression $q_a = q/N$.

Let us evaluate N for real conditions of astrophysical observations. We know from experiment [Ref. 7] that R_θ on the reception aperture of the telescope varies depending on conditions from $R_\theta^{min} = 3$ cm to $R_\theta^{max} = 0.3$ m, and hence we see that for a telescope with $D_T = 1.3$ m, $N = (D_T/R_\theta)^2$ ranges from 1800 to 18. This considerably reduces q_a as compared with q, and as a consequence is quite deterimental to the detection characteristics.

2. Detection Characteristics of Optimum Reception

For distributions (3), (4), the probability of a false alarm is

$$F = \sum_{n=n_0}^{\infty} \frac{A}{n!} e^{-A} = \int_0^A \frac{t^{n_0-1}}{(n_0-1)!} e^{-t}\,dt, \quad n_0 \geqslant 1, \tag{6}$$

and the probability of missing an object is

$$\beta = 1 - D = \sum_{n=0}^{n_0-1} \frac{(A+B)^n}{n!} e^{-(A+B)} = \int_{A+B}^{\infty} \frac{t^{n_0-1}}{(n_0-1)!} e^{-t}\,dt, \quad n_0 \geqslant 1, \tag{7}$$

where D is the probability of correct detection; n_0 is the detection threshold.

The detection characteristics can be calculated both from exact formulas (6) and (7), and from approximate formulas that considerably simplify the calculations. Actually, the case of small probabilities F and β is of interest from the practical standpoint. This case occurs where A and B are fairly large, which is

typical of real conditions of astrophysical observations (see Table 1). In this connection, the asymptotic form of (6) and (7) as A, $B \to \infty$, $q_a = \text{const}$, is most important for practical purposes.

Let us begin our simplification with expression (6) for a false alarm. We note that $n_0 - 1 \geqslant A$, and therefore simultaneously with $A \to \infty$ we must set $n_0 - 1 \to \infty$. Let us introduce the notation $P = (n_0 - 1)/A$. Obviously $P > 1$. We will seek the asymptotic form of (6) at $n_0 - 1 = PA$, $A \to \infty$, $P = \text{const}$. Then

$$F = \int_0^A \frac{t^{PA}}{(PA)!} e^{-t}\, dt = \frac{A^{PA+1}}{(PA)!} \int_0^1 (t^P e^{-t})^A\, dt, \tag{8}$$

where the function $t^P e^{-t}$ increases monotonically on integration segment (0,1) to a maximum of e^{-1}. At large A, the main contribution to the integral is from the values of the function $t^P e^{-t}$ in the vicinity of $t = 1$. Therefore let us use the approximation $(t^P e^{-t})^A = e^{(P \ln t - t)A} \approx e^{-A + (P-1)(t-1)A}$, where the exponential expression is expanded in a Taylor series in the vicinity of the point $t = 1$. Hence

$$\int_0^1 (t^P e^{-t})^A dt \approx e^{-A} \int_0^1 e^{(P-1)(t-1)A} dt = \frac{e^{-A}}{(P-1)A};$$
$$F \approx \frac{A^{PA+1}}{(PA)!} \frac{e^{-A}}{(P-1)A} = \frac{A^{PA}}{(PA)!} \frac{e^{-A}}{P-1}. \tag{9}$$

Then using the Stirling formula, we transform $(PA)! \approx \sqrt{2\pi PA} \cdot (PA)^{PA} e^{-PA}$, and finally get an approximate formula for the probability of a false alarm:

$$F \approx e^{-(P \ln P + 1 - P)A} / (P-1)\sqrt{2\pi PA}. \tag{10}$$

To evaluate the accuracy of approximation (10) and determine the conditions of its applicability, Table 2 presents the results of calculation of F from exact formula (6) and approximate formula (10). We can see that (10) gives a good approximation, and can be used in the case under consideration.

TABLE 2

A	n_0	F (6)	F (10)
1	5	—2,44	—2,28
	6	—3,22	—3,12
	7	—4,08	—3,99
	8	—4,98	—4,90
	9	—5,96	—5,87
3	9	—2,43	—2,31
	10	—3,0	—2,86
	11	—3,53	—3,45
	12	—4,79	—4,73
5	12	—2,28	—2,16
	13	—2,69	—2,60
	15	—3,66	—3,58
	17	—4,71	—4,65
	19	—5,86	—5,81
10	19	—2,15	—2,05
	21	—2,80	—2,74
	23	—3,53	—3,47
	25	—4,33	—4,28
	27	—5,20	—5,17

In an analogous way, we get an approximate formula for the probability of missing an object (7):

$$\beta = \int_{A+B}^{\infty} \frac{t^{PA}}{(PA)!} e^{-t}\, dt =$$
$$= \frac{A^{PA+1}}{(PA)!} \int_{1+q_a}^{\infty} (t^P e^{-t})^A\, dt \approx \tag{11}$$
$$\approx \frac{\exp\left\{-\left[\frac{P}{1+q_a} \ln\left(\frac{P}{1+q_a}\right) + 1 - \frac{P}{1+q_a}\right] A (1+q_a)\right\}}{(1 - P/(1+q_a))\sqrt{2\pi PA}}.$$

The figure shows an example of calculation of detection characteristics $F = f(\beta)$ calculated from formulas (6)-(11) at different A, B and q_a.

From approximate formula

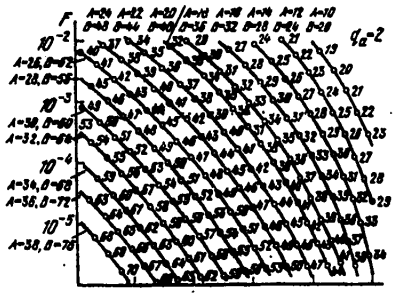

From approximate formula

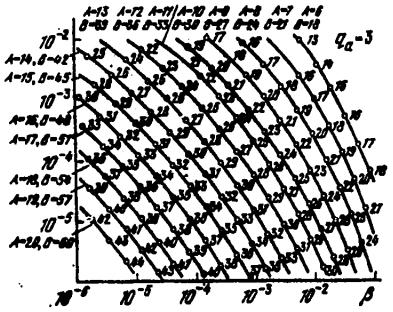

3. Technique for Evaluating the Capabilities of Astrophysics for Detecting Objects Through the Turbulent Atmosphere

Let us consider a method for using these characteristics to evaluate the probability of accurate detection D of an object under real conditions of astrophysical observations. In order to use these characteristics it is first necessary to determine $\bar{n}_c$ and $\bar{n}_\phi = A$ from formulas (1) and (2), or from tables that are analogous to Table 1 for the given conditions of observation. Then for the given D_T and the measured R_θ it is necessary to find the number $N = (D_T/R_\theta)^2$ of spatial regions of coherence of radiation obtained on the reception aperture of the telescope, after which $B = \bar{n}_c/N$ can be determined. From the resultant A, B and q_a, a curve is calculated from (6)-(11), or the appropriate curve is selected from a family of curves like those shown in the figure, and this curve is then used with given F to determine the required threshold of detection and the $D = 1 - \beta$ that results under the given conditions.

To illustrate this procedure, let us consider a numerical example. By using characteristic curves like those shown in the figure, we can readily see that when $D_T = 1.3$ m, $\Delta\lambda = 10$ nm, $T = 0.02$ s, $d = 0.02$ mm, $\lambda = 0.5$ μm, $\tau_{атм} = 0.7$, $\tau_{опт} = 0.5$, $\gamma = 0.1$ for a given probability of false alarm $F = 10^{-5}$ an object of tenth stellar magnitude is detected against the background of a starry sky of eighteenth stellar magnitude in the absence of atmospheric phase distortions ($N = 1$) with probability $D = 0.9997$, and in the presence of weak atmospheric phase distortions ($N = 20$)--with probability $D = 0.92$. This shows that atmospheric phase distortions must be taken into consideration when evaluating the penetrating capacity of ground-based astrophysical observation systems.

Conclusion

Thus under actual conditions of astrophysical observations the quantum statistic of photocounts of optimum reception conforms to a Poisson distribution law. The presence of a turbulent atmosphere characterized by R_θ in front of the reception aperture of a telescope of diameter D_T leads in the resultant distributions to a reduction of $\bar{n}_c$ in the spatial element of resolution of the telescope by a factor of $N = (D_T/R_\theta)^2$ times, and causes appreciable deterioration of the detection characteristic.

BIBLIOGRAPHY

1. Bakut, P. A., Sviridov, K. N. and Ustinov, N. D., KVANTOVAYA ELEKTRONIKA, Vol 6, 1979, p 1932.

2. Bakut, P. A., Sviridov, K. N., Troitskiy, I. N. and Ustinov, N. D., RADIOTEKHNIKA I ELEKTRONIKA, Vol 24, 1979, p 1501.

3. Klimishin, I. A., "Astronomiya nashikh dney" [Astronomy of Our Times], Moscow, Nauka, 1976.

4. Kopeyka, N. S., Bordon'ya, Dzh., TRUDY IIER, Vol 58, No 10, 1970, p 179.

5. Volokhatyuk, V. A., Kochetkov, V. M. and Krasovskiy, R. R., "Voprosy opticheskoy lokatsii" [Problems of Lidar], Moscow, Sovetskoye radio, 1971.

6. Abramenko, A. N. et al., "Televizionnaya astronomiya" [Television Astronomy], Moscow, Nauka, 1974.

7. Schneiderman, A. M. and Karo, D. P., JOURNAL OF THE OPTICAL SOCIETY OF AMERICA, Vol 68, 1978, p 348.

6610
CSO: 1862/124

MATHEMATICS

UDC 519.21:623(024)

QUEUEING SYSTEMS

Moscow SISTEMY MASSOVOGO OBSLUZHIVANIYA in Russian 1980 (signed to press 26 Sep 79) pp 3-4, 188-190

[Annotation, preface and table of contents from book "Queueing Systems: Analysis of Queueing Systems with Blocked Customers in Military Practice", by Aleksandr Ivanovich Lukin, Voyenizdat, 8000 copies, 190 pages]

[Text] Problems of military science are among the most complicated questions that can be investigated only with comprehensive evaluation of both qualitative and quantitative processes that characterize the organization, implementation and support of field operations.

Practical recommendations for sound decision making are given in this book based on methods of queueing theory and mathematical programming with the use of computers.

The book has been written from Soviet and non-Soviet open-source materials. It is intended for persons interested in operations research and logistics.

Preface

It was pointed out in a resolution of the Twenty-Fifth Congress of the Communist Party of the Soviet Union with reference to the CPSU Central Committee's draft of "Major Areas of Development of the National Economy of the USSR for 1976-1980" that one of the main tasks in the area of natural and technical sciences is that of expanding research on theoretical and applied mathematics based on computer technology.

There are great possibilities in military science for using mathematical methods and computers in the analysis of queueing systems.

Queueing theory began its development as one of the areas of probability theory at the turn of the century in application to telephone service. The principles of the theory were laid down in works of the eminent Danish scientist A. K. Erlang.

As is true in general of any theory, the value of queueing theory is in its practical application. The class of problems that can be solved with the methods of

queueing theory grows larger with each passing year. There are extensive possibilities for using these methods in military science.

Under field conditions the need is continuously arising for service on the part of some server that meets this need. In this connection, a problem arises that can be solved by the methods of queueing theory.

For example the queueing concept can be applied to strikes against enemy targets by offensive weapons of various kinds, processing information flows in the period of organization and in the course of battle, in directing units and subunits, and also in the process of supplying troops with equipment and matériel.

This book is being published because there are currently such limited numbers of materials available on the applied aspects of queueing theory. Theoretical works deal mainly with elaboration of fundamental problems in the field of queueing theory, and it is difficult and indeed at times impossible for the military officer to pick out necessary material from these works and put it to practical use. An attempt is made in this book to fill this gap in some measure in a form that is accessible to the military reader.

The author thanks V. V. Tsarin, V. I. Manchevskiy and Yu. T. Protasenya for assistance with the computer calculations.

Contents page

6610
CSO: 1862/118

- END -